

A protease-cleavable liposome for co-delivery of anti-PD-L1 and doxorubicin for colon cancer therapy in mice

Received: 24 June 2023

Accepted: 7 March 2025

Published online: 24 March 2025




Yixuan Liu^{1,2,3}, Ying Xie^{1,2,3}, Yuling Chen^{1,2}, Jialun Duan^{1,2}, Chunjie Bao^{1,2}, Jinling Wang^{1,2}, Hexuan Feng^{1,2}, Mengjie Wang^{1,2}, Yuxin Ren^{1,2}, Peishan Li^{1,2}, Qian Luo^{1,2}, Jiarui Xu^{1,2}, Min Jiang^{1,2}, Yanchen Men^{1,2}, Yang Wu^{1,2}, Jianwei Li^{1,2}, Guiling Wang^{1,2} & Wanliang Lu^{1,2} 

Immune checkpoint blockade therapy using programmed cell death 1 (PD1) or programmed death ligand 1 (PD-L1) has made significant progress in the treatment of advanced cancers, with some patients achieving long-term remission without clinical recurrence. However, only a minority of colon cancer patients respond to the therapy. Here, we report a protease-cleavable anti-PD-L1 antibody liposome, eLipo anti-PD-L1, for enhancing colon cancer therapy. In vivo, eLipo anti-PD-L1 is cleaved by legumain at colon cancer site into pegylated anti-PD-L1 and cancer-homing doxorubicin liposome. Functional assessments show cancer-targeting, legumain-responding, tumor-penetrating, and immune-activating effects, as well as efficacy in treating colon cancer-bearing mice in vivo. Further mechanistic analysis implicates genes related to T cell differentiation and T cell receptor signaling as potential molecular mediators. Lastly, human colorectal cancer tissue evaluations verify expressions of PD-L1 and legumain, hinting a potential translatability. Our study thus suggests that eLipo anti-PD-L1 may be a feasible vector for co-delivery of immunochemotherapy for colon cancer.

Colon cancer is a cancer that develops from the colon part of the large intestine. It is also called bowel cancer or colorectal cancer because the anterior end of the colon is connected to the cecum and the posterior end to the rectum, forming the large intestine¹. Treatment strategies for colorectal cancer mainly consist of surgery, radiation therapy, chemotherapy etc. Colon cancer that is confined within the colon may be curable with surgery, but usually cannot be cured when it has spread widely². The survival depends on how advanced the cancer is, whether all the cancer can be excised with surgery or not, and the patient's health status³. Survival of the patient is directly related to detection and the type of cancer involved, but overall prognosis is poor for the advanced. In developed countries, the five-year survival rate for colorectal cancer is only about a third of patients^{4,5}.

Immune checkpoint blockade therapy using programmed death 1 (PD1) or programmed cell death ligand 1 (PD-L1) has made significant progress in the treatment of advanced malignancies, with some patients achieving long-term remission without clinical recurrence^{6–13}. Evidence shows that PD-L1 is expressed at 89% in colorectal tumor tissues and 5% in normal human tissue cells¹⁴, and the specific rich expression of PD-L1 in colorectal cancer provides a particular advantage for immune checkpoint blockade therapy. Immune checkpoint inhibitors (ICIs) like PD1 antibodies pembrolizumab¹⁵, nivolumab¹⁶, and dostarlimab¹⁷ have been used as first-line therapy for metastatic colorectal cancer (CRC) with defective mismatch repair (dMMR) and/or high microsatellite instability (MSI-H). The results demonstrate that the patients are highly sensitive to these inhibitors (ICIs), leading to

¹State Key Laboratory of Natural and Biomimetic Drugs, School of Pharmaceutical Sciences, Peking University, 100191 Beijing, China. ²Beijing Key Laboratory of Molecular Pharmaceutics and Drug Delivery Systems, School of Pharmaceutical Sciences, Peking University, 100191 Beijing, China. ³These authors contributed equally: Yixuan Liu, Ying Xie  e-mail: luwl@bjmu.edu.cn

significantly longer progression-free survival as compared to chemotherapy. Besides, there are several ICIs like PD-L1 antibodies currently undergoing clinical trials^{18–21}. However, clinical outcome analysis shows that there is no significant difference in overall survival^{22,23}, and there are still limitations in individual variability and duration of therapy response.

The reason for the limited efficacy may come from the immune resistance, in which colorectal cancer with proficient mismatch repair (pMMR) and microsatellite stability (MSS) may be in a “cold” state, such as insufficient activation of immune cells, primary immune dysfunction, and/or irreversible depletion of immune cells. Furthermore, the reason may also be due to the facts that PD1 or PD-L1 antibodies are distributed throughout the body after injection, some antibodies may be eliminated by the mononuclear phagocyte system (MPS) in the blood circulation^{24,25}, and the antibodies are difficult to penetrate into solid cancer²⁶, leading to a lower delivery efficiency of antibody. Even colorectal cancer with dMMR/MSI-H in a “hot” state²³, improving the efficiency of antibody delivery would be able to enhance immune activation, promote immune cell infiltration in the cancer micro-environment, and further improve the efficacy of immunotherapy. Accordingly, how to overcome the immune insufficiency and deliver therapeutic antibodies to colorectal cancer remain the key scientific issues to be solved.

Here, we report a specific protease-cleavable PD-L1 antibody liposome (eLipo anti-PD-L1) for boosting immune checkpoint blockade efficacy of colon cancer. Furthermore, the liposomes can be used to simultaneously deliver chemotherapeutic agent doxorubicin (eLipo anti-PD-L1 dox) for further strengthening the chemoimmunotherapy efficacy. In this construct, the liposome was rationally designed by incorporating a newly synthesized protease-cleavable functional material, consisting of cancer-homing peptide, tumor site specific protease-cleavable peptide, and blood long-circulation liposome membrane material. The PD-L1 antibody (anti-PD-L1) was conjugated onto the liposome while the chemotherapeutic agent (doxorubicin) was encapsulated into the vesicle of liposome.

Anti-PD-L1 usually binds to PD-L1 protein on the surface of a cancer cell, blocks the binding of PD1 on cytotoxic T cell to PD-L1 on cancer cell, thereby playing an anticancer role through activating the signaling pathway of cytotoxic T cell (CTL), and secreting the killer cytokines such as interferon- γ (IFN- γ), and cancer necrosis factor- α (TNF- α). In addition, anti-PD-L1 has a special role in restoring not only killer T cell but also regulatory T (Treg) cell function²⁷. In this study, anti-PD-L1 was conjugated with legumain-specific cleavable liposomes to address the problems of low antibody delivery efficiency and immune response insufficiency in colon tumor site.

Legumain, also known as cysteine protease, is a proteolytic enzyme from C13 peptidase family which hydrolyses the peptide bond using the thiol group of a cysteine residue as a nucleophile²⁸. Under normal physiological condition, legumain is mainly expressed in renal tubules, and assists renal tubular reabsorption^{29,30}. Increasing evidence demonstrates that legumain is overexpressed in the majority of human solid cancers, acting the role in promoting cancer cell migration, invasion and metastases^{31–33}.

In the study, the protease-cleavable liposome is prepared by chemically linking anti-PD-L1 with cancer-homing drug liposome. This construct enables the liposome to deliver both antibody and chemical drug to the deep tissue of colon cancer, where the endogenously rich expressed legumain cleaves the liposome into two parts, including pegylated anti-PD-L1 moiety, and cancer-homing drug liposome moiety, for exerting immune checkpoint blockade and chemotherapy simultaneously. The functional verification and mechanism analysis are performed in vitro and in colon cancer-bearing mice. The expressions of PD-L1 and legumain are verified in human colorectal cancer tissues. The study provides a novel

strategy for boosting immune efficacy of checkpoint blockade antibody and a universal co-delivery vector of colon cancer immunochemotherapy.

Results

Rational design and synthesis of protease-cleavable material

Legumain protease-cleavable material was designed for being selectively cleavable in the colon cancer environment, with a linker for anti-PD-L1 conjugation. The material consisted of lipid liposome material (1,2-distearoyl-sn-glycero-3-phosphoethanolamine, DSPE), cancer homing peptide (CHP, CGNKRTR), protease-cleavable peptide (AAN), and material for blood long-circulation (polyethylene glycol 2000, PEG₂₀₀₀) (Fig. 1a). The synthesis included three main procedures (Fig. 1b). Firstly, DSPE was reacted with suberic anhydride to form carboxylic acid-modified DSPE under catalysis of triethylamine, and then carboxylic acid-modified DSPE was reacted with N-hydroxy succinimide (NHS) to form DSPE-NHS under catalysis of 1-(3-dimethylaminopropyl)-3-ethylcarbodiimide hydrochloride (EDC). Secondly, functional peptide (CHP-AAN-K) was synthesized using CHP, AAN, and K through a solid-phase synthesis, and then reacted with a linear heterobifunctional polyethylene glycol (COOH-PEG₂₀₀₀-Mal) to form CHP-AAN-K-PEG₂₀₀₀-Mal. Finally, DSPE-NHS was covalently linked with CHP-AAN-K-PEG₂₀₀₀-Mal to form eLipid-Mal (DSPE-CHP-AAN-K-PEG₂₀₀₀-Mal).

The identification for DPSE-NHS was performed by ¹H nuclear magnetic resonance (NMR) spectroscopy. The results showed that the characteristic hydroxyl hydrogens (3, δ = 4.18 ppm) and aliphatic hydrogens (1-2, 4-6, δ = 0.88, 1.27, 3.99, 3.5, 2.24 ppm, respectively) in different chemical environments in DSPE and the characteristic carbonyl hydrogens (7, δ = 2.71 ppm) in NHS (Supplementary Fig. 1a) were observed, indicating a successful synthesis of DSPE-NHS. The identification for CHP-AAN-K was performed by liquid chromatography-mass spectrometry (LC-MS). The results showed that the quasi-molecular ions peak [M + H]⁺ signal was found at *m/z* 1332.87 (Supplementary Fig. 1b), which was correspond to the molecular weight of the synthesized peptide product, indicating a successful synthesis of CHP-AAN-K.

The purity of CHP-AAN-K was measured by high-performance liquid chromatography (HPLC) (Supplementary Fig. 1c). The results showed that the purity of CHP-AAN-K reached up to 95.20%, based on the peak area calculation. Furthermore, the identification for CHP-AAN-K-PEG₂₀₀₀-Mal was performed by matrix-assisted laser desorption/ionization time of flight mass spectrometry (MALDI-TOF MS) (Supplementary Fig. 1d). The results showed that the characteristic peak was at *m/z* 3500, which was correspond to the molecular weight of pegylated peptide product, indicating a successful synthesis of CHP-AAN-K-PEG₂₀₀₀-Mal. In addition, the characteristic peak at *m/z* 4800 was correspond to the molecular weight of the final product, indicating a successful synthesis of eLipid-Mal (Supplementary Fig. 1e).

Engineering and characterization of protease-cleavable liposome

Egg phosphatidylcholine, cholesterol, and eLipid-Mal (DSPE-CHP-AAN-K-PEG₂₀₀₀-Mal) were used as the membrane materials (60: 36: 4, mol/mol), and the blank liposome (blank eLipo) was prepared by film dispersion, followed by membrane extrusion³⁴. Anti-PD-L1 was then conjugated onto eLipid-Mal under 4 °C to prepare the protease-cleavable anti-PD-L1 liposome (eLipo anti-PD-L1). Besides, doxorubicin was encapsulated into the blank eLipo using ammonium sulfate gradient method³⁵ and then conjugated with anti-PD-L1 to prepare the protease-cleavable anti-PD-L1 liposome loaded with doxorubicin (eLipo anti-PD-L1 dox). The control liposomes were similarly prepared, including blank Lipo, blank eLipo, Lipo dox, eLipo dox, Lipo anti-PD-L1, and Lipo anti-PD-L1 dox.

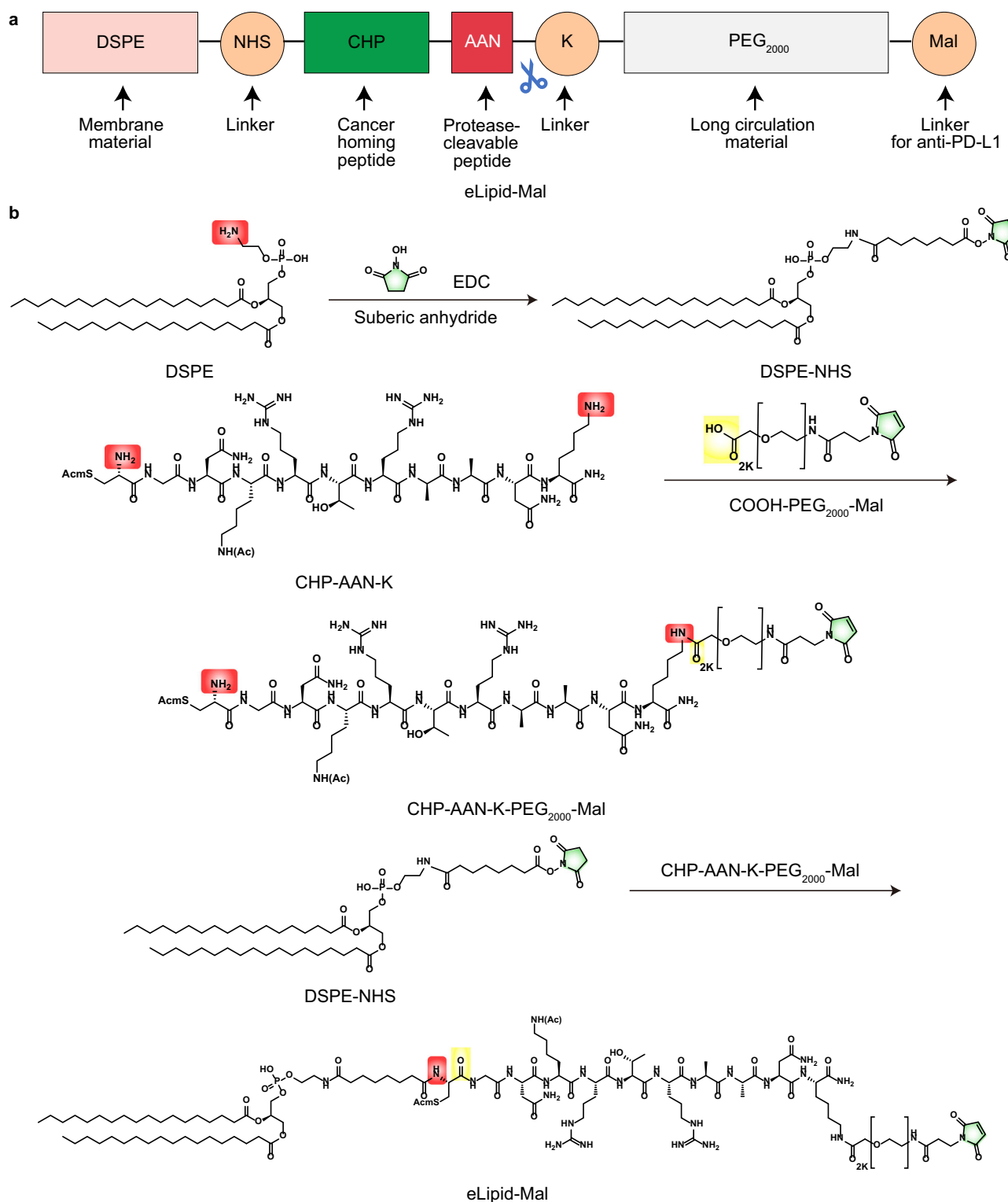


Fig. 1 | Rational design and synthesis of protease-cleavable material. **a** Design for protease-cleavable material. The material was rationally designed for specifically cleaving by legumain protease in the cancer environment and used as a liposome material, mainly consisting of functional segments of lipid material (DSPE), cancer homing peptide (CHP), protease-cleavable fragment (AAN), and long circulation material (PEG₂₀₀₀-Mal). **b** Synthesis route. The protease-cleavable material was synthesized by a three-step process: (1) succinic anhydride was used to carboxylate lipid material DSPE, and then the carboxylated DSPE was reacted with NHS under the

catalysis of EDC to form DSPE-NHS; (2) functional peptide (CHP-AAN-K) was synthesized using CHP, AAN, and K through a solid-phase synthesis, and then was reacted with linear heterobifunctional polyethylene glycol (COOH-PEG₂₀₀₀-Mal) to form CHP-AAN-K-PEG₂₀₀₀-Mal; (3) DSPE-NHS was covalently linked with CHP-AAN-K-PEG₂₀₀₀-Mal to form eLipid-Mal (DSPE-CHP-AAN-K-PEG₂₀₀₀-Mal). DSPE, 1,2-distearoyl-sn-glycero-3-phosphoethanolamine; CHP, cysteine-glycine-asparagine-lysine-arginine-threonine-arginine (CGNKRTR); AAN, alanine-alanine-asparagine; NHS, N-hydroxy succinimide; EDC, 1-(3-dimethylaminopropyl)-3-ethylcarbodiimide hydrochloride; K, lysine.

The mole ratio of eLipid-Mal/anti-PD-L1 was first screened by evaluating anti-PD-L1 coupling efficiency and anti-PD-L1 amount, respectively. The results showed that the coupling efficiency of anti-PD-L1 was decreasing with the increase of eLipid-Mal/anti-PD-L1 ratio (Fig. 2a). Besides, with anti-PD-L1 increasing, the coupling amount was increasing, but decreased at a higher anti-PD-L1 level (eLipid-Mal/anti-PD-L1 = 100:1.53 mol/mol), showing a reverse V-shaped profile (Fig. 2b). According to the binding amount on the liposome (eLipid-Mal/anti-PD-L1, 100:0.46, mol/mol), anti-PD-L1 in each mL liposomes was about 4.4×10^{14} molecules, and anti-PD-L1 on each liposome was about 1.51×10^3 molecules.

The particle size and zeta potential were further evaluated by dynamic light scattering (DLS). The results showed that the eLipid-Mal/anti-PD-L1 ratio did not significantly impact the particle size (Fig. 2c) while reduced electronegativity (Fig. 2d), with the increase of eLipid-Mal/anti-PD-L1 ratio. The reduced absolute value of zeta potential was associated with the combined effects of anti-PD-L1 on the liposomes. Considering that appropriate zeta potential would be conducive to the physicochemical stability of nanoparticles³⁶, and taking into account the above factors, the eLipid-Mal/anti-PD-L1 ratio of 100:0.46 mol/mol was selected for the following study.

The engineered liposomes were characterized by transmission electron microscopy (TEM) and atomic force microscopy (AFM), respectively. The result showed that all liposomes were round and nanosized vesicles (Fig. 2e, f, k, l; Supplementary Fig. 2). The particle size, PDI and zeta potential were further measured by DLS method. The results showed that the particle sizes were approximately 120 nm, having a homogeneous size distribution (123.7 ± 1.7 nm for eLipo anti-PD-L1, $PDI = 0.181 \pm 0.020$; 125.3 ± 1.4 nm for eLipo anti-PD-L1 dox, $PDI = 0.136 \pm 0.013$) and potential distribution (-16.4 mV ± 0.8 for eLipo anti-PD-L1; -17.9 mV ± 2.1 for eLipo anti-PD-L1 dox). In addition, coupling concentration of anti-PD-L1 on various liposomes was approximately 110 μ g/mL (Lipo anti-PD-L1, eLipo anti-PD-L1, Lipo anti-PD-L1 dox, and eLipo anti-PD-L1 dox), and the encapsulation efficacy of doxorubicin in various liposomes was all above 85% (Lipo dox, eLipo dox, Lipo anti-PD-L1 dox, and eLipo anti-PD-L1 dox) (Fig. 2g–j; Supplementary Table 1). The liposomal storage stability was evaluated at 4 °C for a month. The results showed that the liposome formulations (eLipo anti-PD-L1, and eLipo anti-PD-L1 dox) were stable at 4 °C, and the leakage of doxorubicin was kept at 5% or so (Supplementary Fig. 3a–c).

The release profiles of doxorubicin from eLipo anti-PD-L1 dox were further characterized in two media with different pH values (PBS pH 5.5; PBS pH 7.4). The results showed that the cumulative release of doxorubicin in both media was lower than 30% at the initial 2 h. In addition, the cumulative release was 62.15% at 12 h in PBS pH 7.4 medium, and 80.76% at 12 h in PBS pH 5.5 medium (Fig. 2m). These results indicated that doxorubicin was released faster in weak acidic pH medium.

The conjugation of anti-PD-L1 onto liposome was validated by Western blot assay. Immunoglobulin (IgG) molecule is a glycoprotein with a structure similar to the letter Y. The basic structure of the anti-PD-L1 monomer (IgG) consists of two identical half-bodies connected by two disulfide bonds. Each half-body possesses a heavy (H) chain of approximately 60 kDa and a light (L) chain of approximately 25 kDa, which are linked together by disulfide bonds near the carboxy terminus of the light chain. During Western blot assay, the image usually demonstrates two bands at 60 kDa (H chain) and 25 kDa (L chain). In this study, anti-PD-L1 used was a rat IgG2b. The results showed that the Western blot image of anti-PD-L1 exhibited two bands at 60 kDa (H chain) and 25 kDa (L chain). After anti-PD-L1 conjugating with polymer of the liposome through conjugating sulfhydryl group of the antibody with maleimide of the polymer, the Western blot image of Lipo anti-PD-L1 or eLipo anti-PD-L1 displayed a band at 35 kDa, indicating a successful conjugation of anti-PD-L1 with the liposome (Supplementary Fig. 4).

Protease-specific cleavage and binding capability

The expressions of legumain and PD-L1 were evaluated on the colon tissue, the kidney tissue of healthy mice, tumor tissue of subcutaneous colon cancer-bearing mice, and tumor tissue of orthotopic colon cancer-bearing mice by immunofluorescence assay (Fig. 3a). The results showed that both legumain and PD-L1 were the most highly expressed in tumor tissue of the orthotopic colon cancer-bearing mice. At the same time, they were also abundantly expressed in tumor tissue of subcutaneous colon cancer-bearing mice while slightly expressed in normal colorectal tissue and the kidney tissue of healthy mice (Fig. 3b, c).

The expressions of legumain and PD-L1 were further evaluated on the human colorectal cancer microarray which was from 18 females and 32 males for a total of 50 patients with colorectal cancer tissues (from stage I to stage IV) and their corresponding adjacent tissues (Fig. 4a, b). The results demonstrated that PD-L1 was highly expressed in both colorectal cancer tissue (CT) and its adjacent tissue (AT) (Fig. 4c, d). Expression of PD-L1 in CT ($48.2 \pm 26.6\%$) was higher than that in its AT ($34.3 \pm 15.2\%$), and displayed large individual differences in both tissues. Specifically, expression of PD-L1 on cancer cells was observed in 90.0% (9/10) stage I CT (Fig. 4e), 91.7% (22/24) stage II CT (Fig. 4f), 86.7% (13/15) stage III CT (Fig. 4g), and 100% (1/1) stage IV CT. Furthermore, legumain was highly expressed ($10.2 \pm 21.0\%$) in CT but very lowly expressed ($3.1 \pm 8.1\%$) in its AT (Fig. 4h, i). Specifically, expression of legumain on cancer cells was observed in 20.0% (2/10) stage I CT (Fig. 4j), 25.0% (6/24) stage II CT (Fig. 4k), 13.3% (2/15) stage III CT (Fig. 4l), and 0% (0/1) stage IV CT. Since the only one stage IV sample (g2) had an invalid corresponding AT sample (g7), no matched comparison was made between stage IV CT and AT.

Besides, the expressions of neuropilin-1 (NRP-1) receptor and PD-L1 were further evaluated on the colon cancer CT-26 cells (Supplementary Fig. 5a, f), MC-38 cells (Supplementary Fig. 5b, g), CMT-93 cells (Supplementary Fig. 5c, h), and Caco-2 cells (Supplementary Fig. 5d, i) by flow cytometry. The results demonstrated that both CT-26 and CMT-93 cells highly expressed NRP-1 receptor, while MC-38 and Caco-2 cell expressed very little NRP-1 receptor (Supplementary Fig. 5e). Meanwhile, CT-26, MC-38, and CMT-93 cells highly expressed PD-L1 protein, while Caco-2 cells expressed very little PD-L1 protein (Supplementary Fig. 5j). As colon cancer CT-26 cells highly expressed both NRP-1 receptor and PD-L1 protein, it was selected for establishing the orthotopic colon cancer-bearing mice model.

Legumain-specific cleavage ability was determined with fluorescent peptide substrate (CBZ-AAN-AMC)^{37,38}, as the substrate itself had no fluorescence signal, but once it was cleaved by legume protease, the free AMC restored its fluorescence property and the fluorescence was detectable. In the study, the substrate buffer solution (50 mM MES, 250 mM NaCl, pH 5.5) was used as a blank control. The results showed that the substrate exhibited obvious fluorescence when incubated with legumain-containing buffer, while the substrate did not display any fluorescence when incubated the buffer solution containing legumain and RR-11a (a specific inhibitor of legumain)^{39,40}. For verifying legumain-specific cleavage capability in tumor tissue, an ELISA assay was used to quantify legumain level in the orthotopic colon cancer tissue. The results showed that legumain was 66.25 ng/L in the orthotopic colon cancer tissue, exhibiting abundant expression. Besides, for validating legumain-specific cleavage capability, the commercially available legumain, and the orthotopic colon cancer tissue homogenates were also incubated with CBZ-AAN-AMC substrate, respectively. The results showed that both treatments were effective in cleaving the AAN motif on eLipo anti-PD-L1, and cancer tissue homogenate displayed a comparable cleavage ability to commercial legumain added (2 ng/ μ L). In addition, when incubating temperature was dropped to 4 °C, the cleavage ability was inhibited obviously, exhibiting a temperature-dependent cleavage mode (Fig. 3d, e; Supplementary Fig. 6a, b).

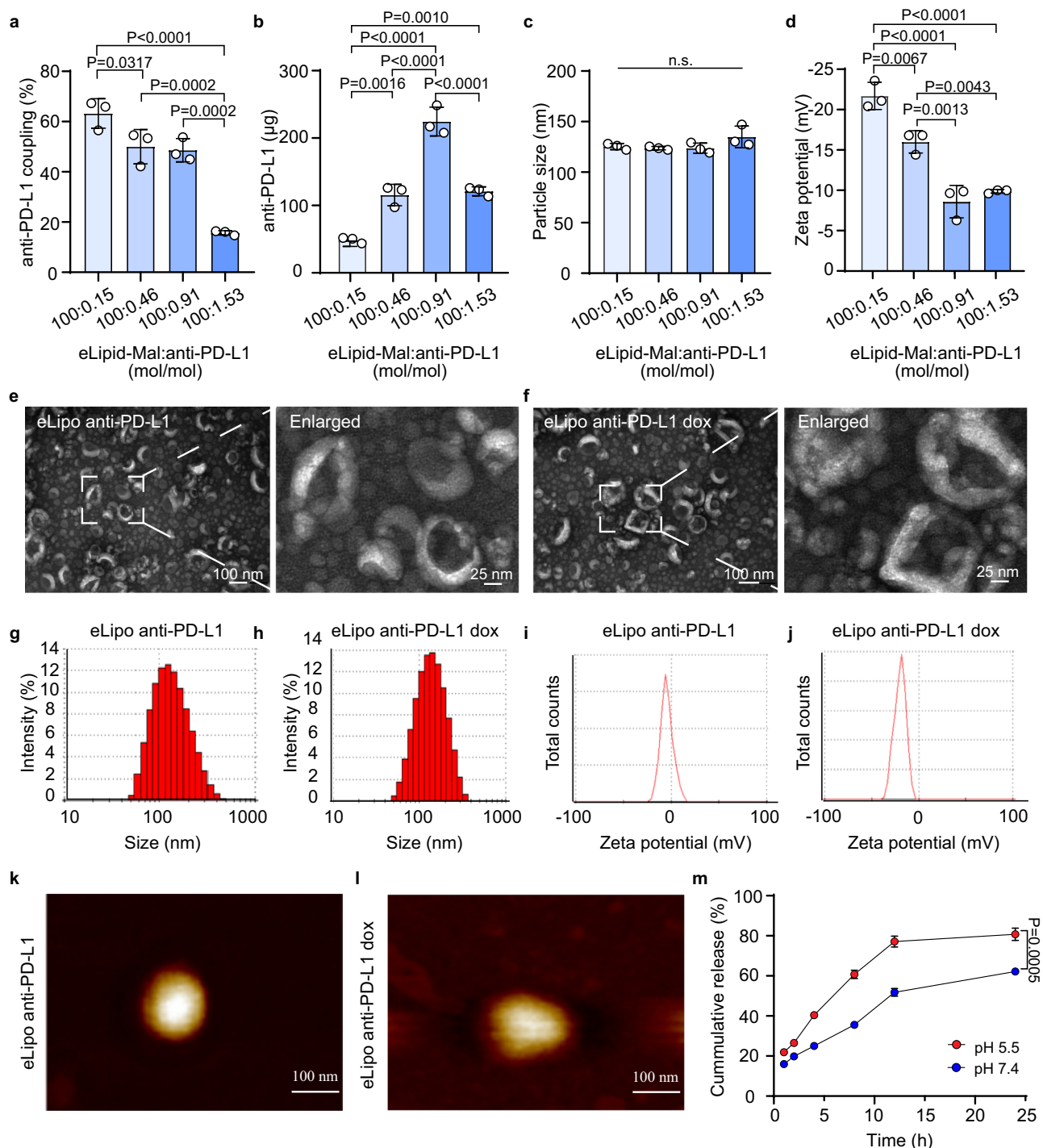


Fig. 2 | Engineering and characterization of protease-cleavable liposome.

a–d Conjugation optimization. **a** anti-PD-L1 coupling efficiency. The ratio of eLipo/anti-PD-L1 was optimized by bicinchoninic acid (BCA) protein assay for evaluating the coupling efficiency of anti-PD-L1. **b** Anti-PD-L1 amount. The ratio of eLipo/anti-PD-L1 was optimized by protease-linked immunosorbent assay (ELISA) for evaluating the amount of coupled anti-PD-L1. **c** Particle size. The ratio of eLipo/anti-PD-L1 was optimized by dynamic light scattering (DLS) for evaluating the particle size. **d** Zeta potential values. The ratio of eLipo/anti-PD-L1 was optimized by DLS for evaluating the zeta potential values ($n = 3$ independent experiments). **e, f** TEM images. The study was performed by transmission electronic microscopy (TEM). **e** eLipo anti-PD-L1; **f** eLipo anti-PD-L1 dox. Scale bar, 100 nm. Enlarged bar, 25 nm. The experiments were repeated four times independently with similar results. **g, h** Particle size distribution. The study was performed by DLS. **g** eLipo anti-PD-L1; **h** eLipo anti-PD-L1 dox. The experiments were repeated four times independently with similar results. **i, j** Zeta potential

distribution. The study was performed by DLS. **i** eLipo anti-PD-L1; **j** eLipo anti-PD-L1 dox. The experiments were repeated four times independently with similar results. **k, l** AFM images. The study was performed by atomic force microscopy (AFM). **k** eLipo anti-PD-L1; **l** eLipo anti-PD-L1 dox. Scale bar, 100 nm. The experiments were repeated four times independently with similar results. **m** Doxorubicin release. Doxorubicin (dox) release from eLipo anti-PD-L1 dox was measured under different pH conditions (PBS, pH 5.5, and PBS, pH 7.4) ($n = 3$ independent experiments). eLipo anti-PD-L1 represents legumain protease-cleavable anti-PD-L1 liposome, where PD-L1 antibody is conjugated with protease-cleavable liposome; eLipo anti-PD-L1 dox represents legumain protease-cleavable anti-PD-L1 plus dox liposome, where doxorubicin (dox) is encapsulated into the vesicle of eLipo anti-PD-L1. Data are shown as the mean \pm SD. Statistical significance (in **a–d**) was determined by a one-way ANOVA test, followed by a Turkey multiple comparisons post test. Statistical significance (in **m**) was determined by a two-tailed unpaired t test. Source data are provided as a Source Data file.

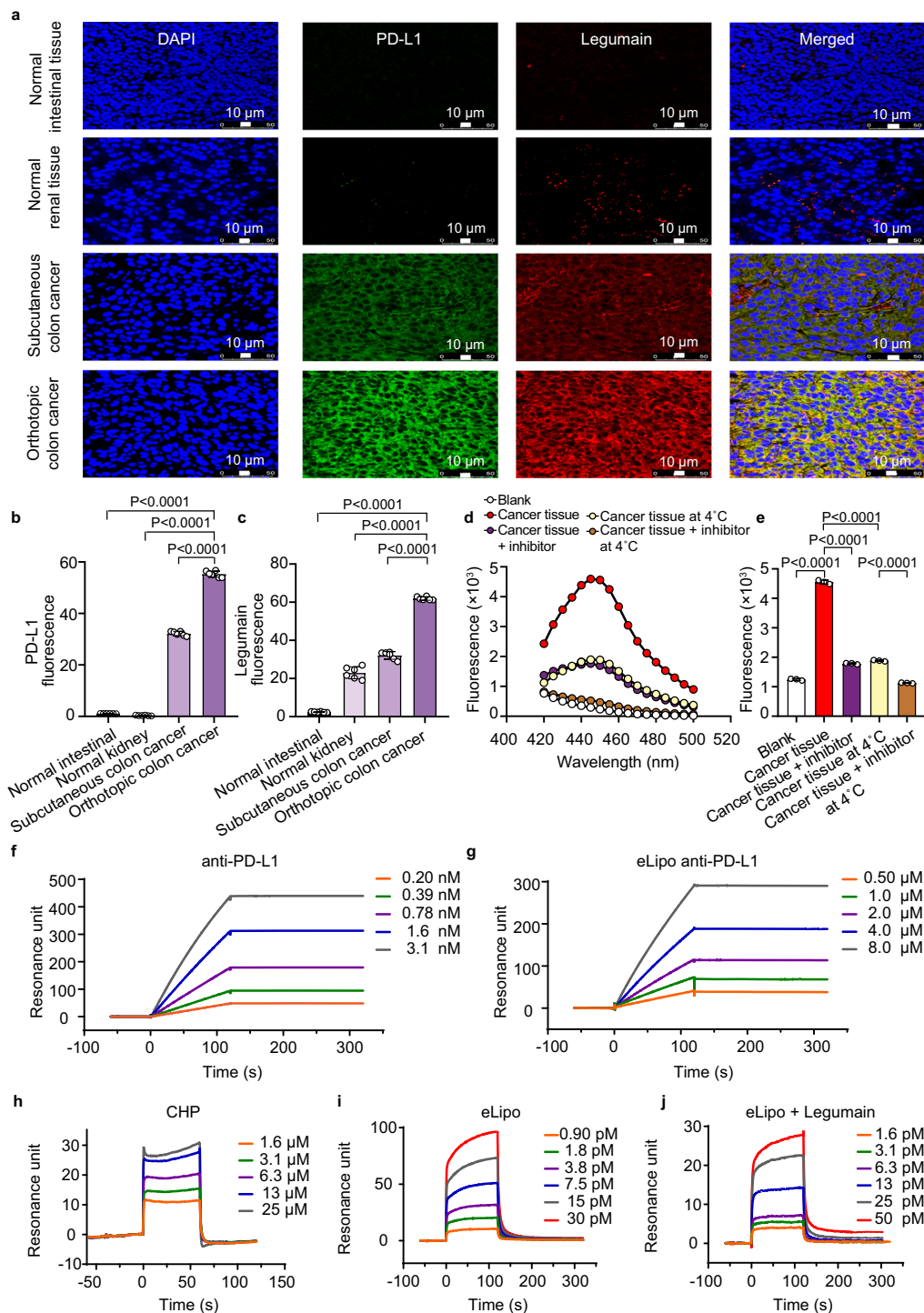


Fig. 3 | Specific protease cleavage and binding capability. **a** Expressions of PD-L1 and legumain in different tissues. The expressions of PD-L1 and legumain were observed by confocal laser scanning microscopy (CLSM) on the normal intestinal tissues of *BALB/c* mice, normal renal tissues of *BALB/c* mice, tumor tissues of subcutaneous colon cancer-bearing *BALB/c* mice, and tumor tissues of orthotopic colon cancer-bearing *BALB/c* mice ($n = 6$ mice). Blue channel (4',6-diamidino-2-phenylindole, DAPI) indicates nucleus; green channel, Alexa Fluor 488 indicates the expression of PD-L1; red channel (Cy3, cyanine 3) indicates the expression of legumain. Scale bar, 10 μm . **b**, **c** Quantification of PD-L1 and legumain. The fluorescence values of above samples were quantified by CLSM ($n = 6$ mice). **b** PD-L1; **c** Legumain. The images were quantified by LAS X Life Science microscopy software. **d**, **e** Specific protease cleavage by orthotopic colon cancer tissue. The specific cleavage ability of the protease-cleavable liposomes was indicated by the fluoro-genic peptide substrate (CBZ-AAN-AMC) in cancer tissue homogenate-containing buffer solution (50 mM MES, 250 mM NaCl, pH 5.5), and measured (excitation at

353 nm; emission at the range of 420–500 nm) by a microplate reader ($n = 3$ independent experiments). **d** Specific protease cleavage profiles; **e** Quantification for specific protease cleavage. Legumain-specific inhibitor, RR-11a; control, CBZ-AAN-AMC buffer solution (50 mM MES, 250 mM NaCl, pH 5.5). **f**, **g** Binding between anti-PD-L1 and PD-L1. The binding ability was verified by surface plasmon resonance (SPR). **f** Binding between anti-PD-L1 and PD-L1; **g** Binding between eLipo anti-PD-L1 and PD-L1. Both equilibrium dissociation constants (K_D) were not detectable due to the strong binding. **h**–**j** Binding between CHP and free NRP-1 protein. The binding ability was verified by SPR. **h** Binding between CHP and free NRP-1 protein. K_{D1} , 6.49×10^{-6} M. **i** Binding between eLipo and free NRP-1 protein. K_{D2} , 1.4×10^{-11} M. **j** Binding between eLipo and free NRP-1 protein in the presence of legumain. K_{D3} , 1.96×10^{-11} M. Data are shown as the mean \pm SD. Statistical significance (in **b**, **c**, **e**) was determined by a one-way ANOVA test, followed by a Turkey multiple comparisons post-test. Source data are provided as a Source Data file.

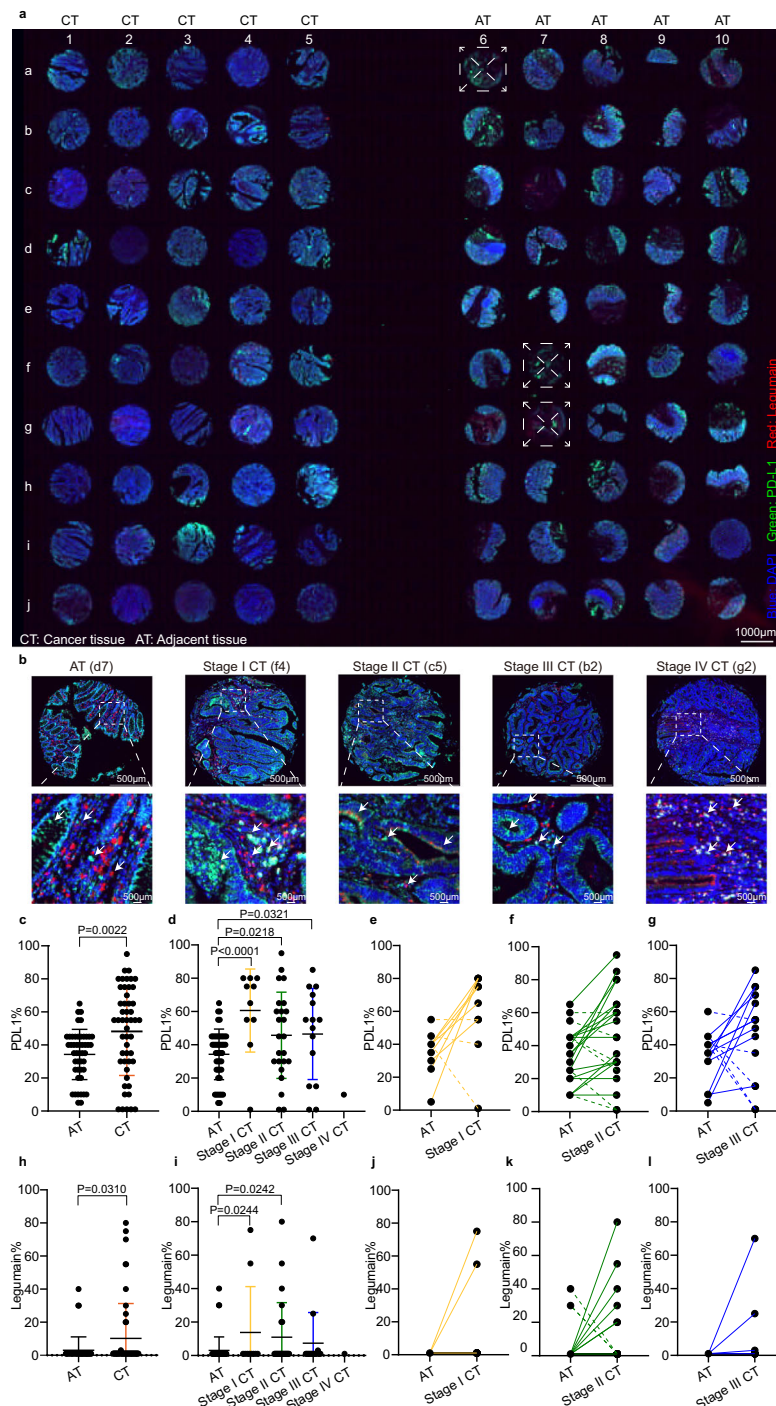


Fig. 4 | Expressions of PD-L1 and legumain in human colorectal cancer and its adjacent tissue. **a** Immunofluorescence for colorectal cancer tissue and adjacent tissue. The column (1, 2, 3, 4, or 5) represents colorectal cancer tissue (CT), and the column (6, 7, 8, 9, or 10) represents its corresponding adjacent tissue (AT). White dashed rectangles, invalid staining; blue channel (DAPI), nucleus; green channel (Alexa Fluor 488), PD-L1; red channel (Cy3), legumain. Scale bar, 1000 μm. **b** Representative images. d7 (AT), membrane of glandular epithelial cell, weak green light; membrane of immune cell, strong green light; glandular epithelial cell, not exhibiting red fluorescence; cytoplasm of immune cell, red fluorescence. f4 (c5, b2 or g2, CT), membrane of colorectal cancer cell, strong green fluorescence; cytoplasm of cancer cell, strong red fluorescence; immune cell, the same as cancer cell. Yellow fluorescence, co-expressions of PD-L1 and legumain. Scale bar, 500 μm. **c** Overall expression of PD-L1 (AT, $n = 47$ patients; CT, $n = 50$ patients). **d** Expression of PD-L1 in AT and varying stage CT (AT, $n = 47$ patients; stage I CT, $n = 10$ patients; stage II CT, $n = 24$ patients; stage III CT, $n = 15$ patients; stage IV CT, $n = 1$ patient). **e** Expression of PD-L1 by matching stage I CT with its AT (10 pairs of valid matched

specimens). **f** Expression of PD-L1 by matching stage II CT with its AT (22 pairs of valid matched specimens). **g** Expression of PD-L1 by matching stage III CT with its AT (15 pairs of valid matched specimens). The two paired specimens are connected by solid (indicating CT PD-L1 \geq AT PD-L1) or dashed line (indicating CT PD-L1 < AT PD-L1). **h** Overall expression of legumain in AT and in CT (AT, $n = 47$ patients; CT, $n = 50$ patients). **i** Expression of legumain in AT and in varying stage CT (AT, $n = 47$ patients; stage I CT, $n = 10$ patients; stage II CT, $n = 24$ patients; stage III CT, $n = 15$ patients; stage IV CT, $n = 1$ patient). **j** Expression of legumain by matching stage I CT with its AT (10 pairs of valid matched specimens). **k** Expression of legumain by matching stage II CT with its AT (22 pairs of valid matched specimens). **l** Expression of legumain by matching stage III CT with its AT (15 pairs of valid matched specimens). The two paired specimens are connected by solid (indicating CT legumain \geq AT legumain) or dashed line (indicating CT legumain < AT legumain). Data are shown as the mean \pm SD. Statistical significance (in **c**, **d**, **h**, **i**) was determined by a two-tailed unpaired t test. Source data are provided as a Source Data file.

The binding ability between anti-PD-L1 and PD-L1 protein was confirmed by surface plasmon resonance (SPR) assay. The results showed that both anti-PD-L1 and eLipo anti-PD-L1 exhibited strong affinity to PD-L1 protein, and shared a similar binding profile without dissociation (Fig. 3f, g). Besides, the chemical coupling of anti-PD-L1 with the liposome did not affect the bioactivity of anti-PD-L1 binding to PD-L1 protein. The binding ability between cancer homing peptide (CHP) and NRP-1 protein was also verified by SPR assay. The results showed that the free CHP peptide had obvious affinity to NRP-1 protein, followed by an immediate dissociation with a high equilibrium dissociation constant ($K_{D1} = 6.49 \times 10^{-6}$ M) (Fig. 3h). The CHP peptide on eLipo exhibited a strong affinity to NRP-1 protein, but followed by a fast dissociation with a low equilibrium dissociation constant ($K_{D2} = 1.4 \times 10^{-11}$ M) (Fig. 3i). In the presence of legumain, the CHP peptide conjugated on the eLipo also demonstrated a strong affinity to NRP-1 protein, but followed by a quick dissociation with a comparable equilibrium dissociation constant ($K_{D3} = 1.96 \times 10^{-11}$ M) (Fig. 3j). These results indicated that CHP can bind to NRP-1 protein, and when CHP was coupled to eLipo, the binding ability was further enhanced. The results suggested that the fast dissociation of the eLipo with surface NRP-1 receptor would be beneficial for the subsequent endocytosis of the cleaved liposome by the cancer cells⁴¹.

Targeting accumulation and deep penetration capability

Orthotopic colon cancer bearing mice (Supplementary Fig. 7a, b) were used for validating the targeting performance. The targeting distribution of eLipo anti-PD-L1 dox was separately evaluated from two aspects, including the pegylated anti-PD-L1 part and the liposome part, considering the cleavage of eLipo anti-PD-L1 in vivo. To study the targeting ability of the pegylated anti-PD-L1 part, a fluorescent probe (sulfo-cyanine 5.5 NHS ester, Cy5.5) was conjugated with anti-PD-L1 for labeling anti-PD-L1, Lipo anti-PD-L1, and eLipo anti-PD-L1, respectively. The above formulations were intravenously injected into the orthotopic colon cancer-bearing mice. PBS (pH 7.4) and free Cy5.5 were used as the controls. The targeting ability of all the formulations were observed at a fixed time-point (2, 4, 8, 12, 24, 48 h) by imaging Cy5.5 fluorescence in vivo. The results showed that both Lipo anti-PD-L1 and eLipo anti-PD-L1 had evident blood long circulation effect compared with anti-PD-L1 (Fig. 5a; Supplementary Fig. 8). Besides, the distributions of the formulations were further observed on the ex vivo tissues at 48 h, and the results showed that both Lipo anti-PD-L1 and eLipo anti-PD-L1 were significantly accumulated in the tumor site of the orthotopic colon cancer-bearing mice, indicating a significant cancer targeting effect. Moreover, they also distributed in the major organ tissues like liver, spleen, lung, and kidney, except for heart. In contrast, anti-PD-L1 had only less distribution in the tumor tissue and minimal in other organs (Fig. 5b). The quantification analysis further demonstrated the results of the imaging observations (Fig. 5c).

For studying the targeting ability of the liposome part, a fluorescent membrane probe (1,1-dioctadecyl-3,3,3,3-tetramethylindotricarbocyanine iodide, DiR) was encapsulated into the vesicle of liposome for labeling Lipo, eLipo, Lipo anti-PD-L1 and eLipo anti-PD-L1, respectively. PBS (pH 7.4) and free DiR were used as the controls. The targeting ability of all the formulations were observed by imaging DiR fluorescence at the same fixed time-points as above. The results showed that all liposomes (Lipo, eLipo, Lipo anti-PD-L1 and eLipo anti-PD-L1) had significant blood long circulation effect compared with free DiR (Supplementary Fig. 9a). Moreover, the distributions of the formulations were further observed on the ex vivo tissues at 48 h, and the results showed that both eLipo and eLipo anti-PD-L1 were most significantly accumulated in the tumor site of the orthotopic colon cancer-bearing mice, indicating a significant cancer targeting effect. Besides, Lipo and Lipo anti-PD-L1 were also somewhat accumulated in the tumor site (Supplementary Fig. 9b). Besides, we further validated the pharmacokinetic profiles

of eLipo anti-PD-L1 dox compared with free doxorubicin. The pharmacokinetic profiles (Supplementary Fig. 10) and pharmacokinetic parameters (Supplementary Table 3) were analyzed by HPLC-MS/MS. The results showed that eLipo anti-PD-L1 dox exhibited a significant long-circulatory blood exposure in the rats.

For further understanding the amount of anti-PD-L1 in colon tumor site, a separate enzyme linked immunosorbent (ELISA) assay was performed by quantifying anti-PD-L1 in the tumor site of the orthotopic colon cancer-bearing mice. Various formulations (anti-PD-L1, Lipo anti-PD-L1, eLipo anti-PD-L1) were intravenously injected into the colon cancer-bearing mice at a dose of 2.3 mg anti-PD-L1/kg at day 7, 9, and 11, respectively. PBS (pH 7.4) was used as the blank control. All colon cancer masses were isolated at day 14 for accurate quantification. The results showed that the anti-PD-L1 concentrations in the colon cancer masses of anti-PD-L1, Lipo anti-PD-L1, and eLipo anti-PD-L1 treated mice were 106.74 ± 0.03 ng/g, 88.86 ± 0.04 ng/g, and 124.06 ± 0.04 ng/g, respectively (Fig. 5d).

For evaluating the penetration ability of protease-cleavable liposome, fluorescence probe Cy5.5 was conjugated with anti-PD-L1 to label anti-PD-L1, Lipo anti-PD-L1, and eLipo anti-PD-L1, respectively. The formulations were applied to the in vitro colon cancer spheroids, and observed by confocal laser scanning microscopy (CLSM). The results from the vertical view and the layer-by-layer scanning showed that eLipo anti-PD-L1 displayed the strongest penetration effect compared with the others, in both qualitative observation (Fig. 5e; Supplementary Fig. 11a, b) and quantitative assessment (Fig. 5f), indicating a significant deep penetration ability into the solid cancer spheroids.

Furthermore, various formulations (dox, Lipo dox, eLipo dox, Lipo anti-PD-L1 dox, and eLipo anti-PD-L1 dox) were used for evaluating the in vitro cellular uptake of colon cancer cells by adding legumain protease. The uptake was studied by using the high content imaging system. The fluorescence of doxorubicin was used to indicate the uptake of liposome, while the fluorescence of Hoechst 33342 dye was used to indicate the cell nucleus. The results showed that eLipo anti-PD-L1 dox exhibited the most significant uptake effect by colon cancer cells compared with other controls, in both qualitative observation (Fig. 5g; Supplementary Figs. 12, 13a, 14a, 15a) and quantitative assessment (Fig. 5h; Supplementary Figs. 13b, 14b, 15b), indicating an enhanced cellular uptake ability in the colon cancer cells. The difference in uptake efficiency between the different cell lines may be due to the difference in NRP-1 and PD-L1 protein expression levels on each cell line.

Fluorescence resonance energy transfer (FRET) assay was performed to investigate the binding interaction between anti-PD-L1 and PD-L1 protein within a co-culture system of colon cancer CT-26 cells with T cells. Furthermore, the binding effect was detected on colon cancer MC-38 cells, colon cancer CMT-93 cells, and colon cancer Caco-2 cells, respectively. The results showed that T cells exhibited high PD-L1 expression as well (Supplementary Fig. 16a). As a result, there existed a strong FRET effect between T cell and anti-PD-L1 (Supplementary Fig. 16b, c). Besides, the FRET effect between colon cancer cell (CT-26, MC-38, and CMT-93) and anti-PD-L1 was also observed (Supplementary Figs. 16b, c, 17), respectively, suggesting a specific binding effect between anti-PD-L1 and these cell types. However, the PD-L1 null Caco-2 cells rarely exhibited FRET effect (Supplementary Fig. 17), indicating that eLipo anti-PD-L1 hardly binds with Caco-2 cell due to low expression of PD-L1 on Caco-2 cell.

Activation mechanism of immune response

The activation mechanism of immune response was firstly evaluated on the gene regulation aspect, in which CD8⁺ T cells were co-cultured with colon cancer CT-26 cells, followed by treating with various formulations (PBS pH 7.4, eLipo anti-PD-L1 and eLipo anti-PD-L1 dox) for transcriptome sequencing analysis, respectively. The results showed that eLipo anti-PD-L1 caused significant changes of 1004 differentially

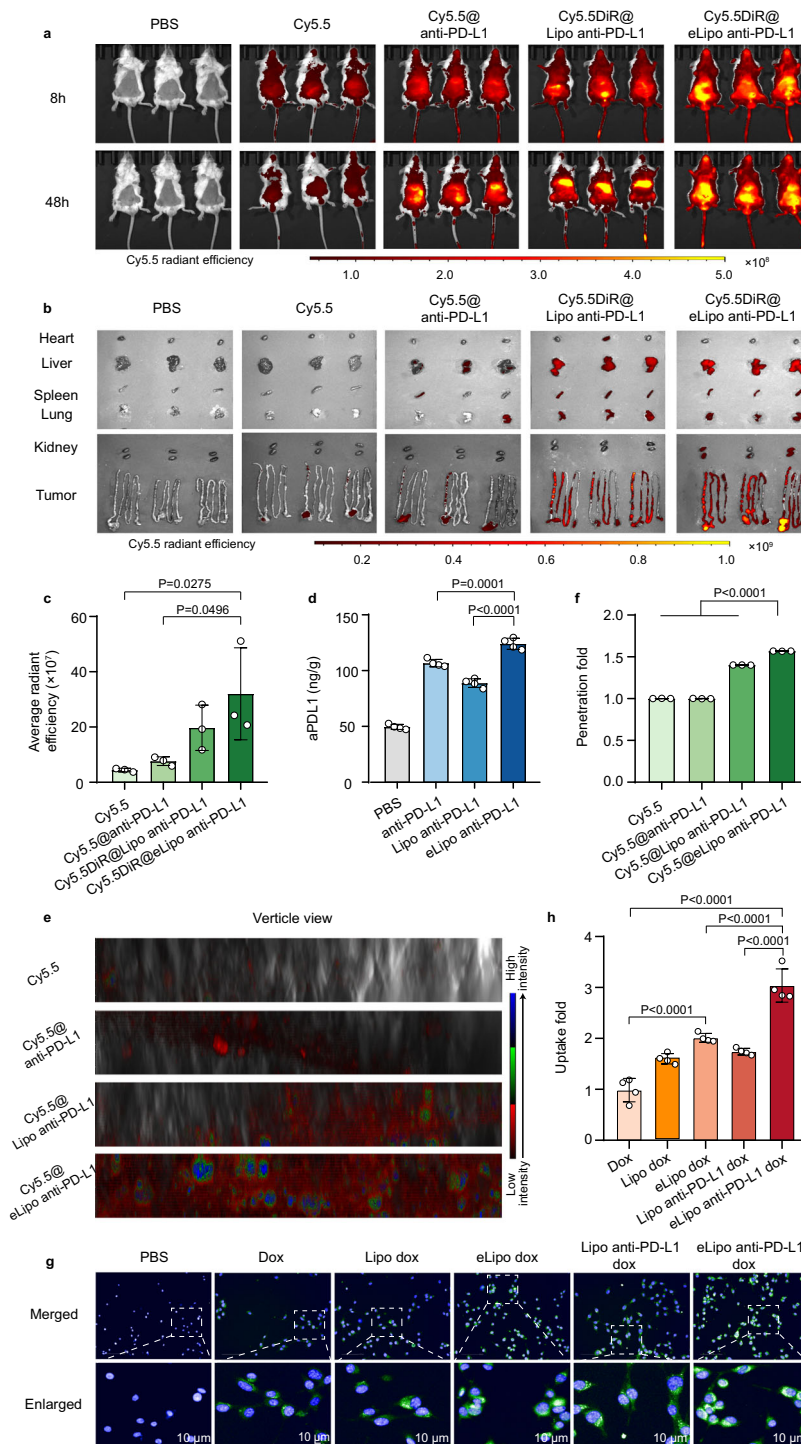


Fig. 5 | Targeting accumulation and deep penetration. **a–c** Targeting ability in cancer-bearing mice. The targeting accumulation was verified from two aspects including fluorescence labeled anti-PD-L1 and fluorescence labeled liposome in the orthotopic colon cancer-bearing mice ($n = 3$ mice). **a** Imaging in vivo. **b** Imaging ex vivo. **c** Quantification of imaging ex vivo. The images were quantified by the Living Image software on IVIS spectrum imaging system. **d** anti-PD-L1 quantification in colon tumor tissue. The measurement was performed on orthotopic colon cancer-bearing mice ($n = 4$ mice). Various formulations (PBS pH 7.4, anti-PD-L1, Lipo anti-PD-L1, and eLipo anti-PD-L1; each dosing, 2.3 mg anti-PD-L1/kg) were intravenously injected at day 7, 9 and 11 since the inoculation and cancer masses were isolated at day 14 for quantifying anti-PD-L1 by ELISA. **e, f** Deep penetration in colon cancer spheroids. The deep penetration was performed on colon cancer spheroids ($n = 3$ independent experiments). **e** CLSM observation. Various formulations (Cy5.5, Cy5.5@anti-PD-L1, Cy5.5DiR@Lipo anti-PD-L1, and Cy5.5DiR@eLipo anti-PD-L1)

were applied to the spheroids for 3 h, and observed by CLSM. **f** Quantification. The images were quantified by the LAS X Life Science microscopy software on CLSM system. **g, h** Targeting uptake by colon cancer cells. The targeting cellular uptake was performed on colon cancer cells ($n = 4$ independent experiments). **g** High content imaging. Various formulations (PBS pH 7.4, dox, Lipo dox, eLipo dox, Lipo anti-PD-L1 dox, and eLipo anti-PD-L1 dox) were applied to colon cancer cells in the presence of legumain (2 ng/ μL) for 2 h, and stained with Hoechst 33342. The cellular uptake was measured with the high content imaging system. Blue channel (Hoechst 33342) indicates nucleus; green channel indicates dox. Scale bar, 10 μm . **h** Quantification. The images were quantified by the high content imaging system. Data are shown as the mean \pm SD. Statistical significance (in **c, d, f, h**) was determined by a one-way ANOVA test, followed by a Turkey multiple comparisons post-test. Source data are provided as a Source Data file.

expressed genes, in which 322 genes were upregulated, and 682 genes were downregulated, as compared with the blank control. Moreover, eLipo anti-PD-L1 dox resulted in significant changes of 1186 differentially expressed genes, in which 489 genes were upregulated, and 697 genes were downregulated. In these altered differentially expressed genes, 115 immune relevant genes were identified, including the remarkably up-regulated immune-activation genes (*Cd14*, *Tnfrsf1b*, *Tapbp*, *Cd81*, *Bst2*, *H2-K1*, *Ticam1*, *Il33*, *Cd3g*, etc.; Fig. 6a). The results from the gene ontology (GO) enrichment revealed that the changed genes were mainly involved in promoting interferon-gamma production, enhancing T cell differentiation, activating immune response, regulating T cell receptor signaling pathway, and increasing tumor necrosis factor receptor binding (Fig. 6b). In addition, the results from Reactome enrichment analysis exhibited that the altered genes were mainly enriched in the pathways relevant to innate immune system, adaptive immune system, T cell receptor signaling pathway, cytokine signaling immune system, MHC class II antigen presentation, and CD28 co-stimulation (Fig. 6c).

The activation mechanism was further verified on the immune cells from tumor tissue of the orthotopic colon cancer-bearing mice after treatments of various formulations (PBS pH 7.4, anti-PD-L1, Lipo anti-PD-L1, and eLipo anti-PD-L1; Fig. 6d), respectively. The subpopulations of the immune cells were measured by flow cytometry. The results showed that eLipo anti-PD-L1 significantly increased the percentages of mature dendritic cells (CD80⁺CD86⁺ cells; Fig. 6e), cytotoxic T lymphocytes (CTLs, CD8⁺ T cells; Fig. 6f), and regulatory T lymphocytes (Treg cells, CD4⁺FOXP3⁺ T cells; Fig. 6g) in the tumor tissue. The further comparison demonstrated that eLipo anti-PD-L1 significantly enhanced the ratio of CTLs to Treg cells (Fig. 6h). These results indicated that eLipo anti-PD-L1 played a remarkable activation role in the tumor site of the orthotopic colon cancer-bearing mice.

Besides, the activation mechanism was also evaluated on the immune cells from spleen of the orthotopic colon cancer-bearing mice by flow cytometry. The results showed that eLipo anti-PD-L1 remarkably increased the percentages of cytotoxic T lymphocytes (CTLs, CD8⁺ T cells; Fig. 6i), TNF- α expression in CD8⁺ T lymphocytes (Fig. 6j), and IFN- γ expression in CD8⁺ T lymphocytes (Fig. 6k), while restored the exhausted T lymphocytes (PD1^{hi}CD8⁺ T lymphocytes; Fig. 6l). These results indicated that eLipo anti-PD-L1 acted a significant activation role in the spleen of the orthotopic colon cancer-bearing mice.

In addition, CD8⁺ T lymphocytes expression was verified on the tumor tissue of the orthotopic colon cancer-bearing mice by immunofluorescence assay. The results showed eLipo anti-PD-L1 significantly enhanced the CD8⁺ T lymphocytes expression in the tumor tissue, in both qualitative observation (Fig. 6m) and quantitative assessment (Fig. 6n).

Therapeutic efficacy in the colon cancer-bearing mice

The inhibitory effect on tumor growth was performed on the orthotopic colon cancer-bearing mice after treatment with various formulations (PBS pH 7.4, anti-PD-L1, Lipo anti-PD-L1, eLipo anti-PD-L1, dox, Lipo dox, eLipo dox, Lipo anti-PD-L1 dox, and eLipo anti-PD-L1 dox; Fig. 7a), respectively. The results showed that eLipo anti-PD-L1 had evident stronger inhibitory efficacy on tumor growth compared with the controls (PBS pH 7.4, anti-PD-L1 and Lipo anti-PD-L1). By incorporating the anticancer drug, eLipo anti-PD-L1 dox demonstrated the most significant inhibitory effect on tumor growth compared with others (PBS pH 7.4, anti-PD-L1, Lipo anti-PD-L1, eLipo anti-PD-L1, dox, Lipo dox, eLipo dox, and Lipo anti-PD-L1 dox) (Fig. 7b; Supplementary Fig. 18a, b).

The body weight and blood biochemical indicators were investigated to evaluate the preliminary safety. The results showed that both eLipo anti-PD-L1 and eLipo anti-PD-L1 dox had no significant effects on

body weight, while caused minute or various degrees of weight loss in other groups, with free dox being the most significant (Fig. 7c). Similarly, blood biochemical indices showed that eLipo anti-PD-L1 and eLipo anti-PD-L1 dox did not affect aspartate aminotransferase (AST; Fig. 7d) and albumin (ALB; Fig. 7e), suggesting that both formulations were safe for intravenous injection. Besides, anti-PD-L1 containing formulations did not affect blood urea concentration (Supplementary Fig. 19). The results from HE staining and Masson staining showed that there was no obvious organic injury and no abnormal renal fibrosis in kidneys, suggesting that anti-PD-L1 containing formulations did not affect normal kidney physiology and function (Supplementary Fig. 20a, b).

The survival curve was further evaluated on the luciferase-labeled ^{luc}CT-26 orthotopic colon cancer-bearing mice after treatment with various formulations (PBS pH 7.4, anti-PD-L1, Lipo anti-PD-L1, eLipo anti-PD-L1, dox, Lipo dox, eLipo dox, Lipo anti-PD-L1 dox, and eLipo anti-PD-L1 dox; Fig. 7f), respectively. The results demonstrated that both eLipo anti-PD-L1 and eLipo anti-PD-L1 dox significantly extended the lifetime of the colon cancer-bearing mice compared with other controls (PBS pH 7.4, aPDL1, Lipo anti-PD-L1, eLipo anti-PD-L1, dox, Lipo dox, eLipo dox, and Lipo anti-PD-L1 dox; Fig. 7g). Furthermore, the comparison showed that eLipo anti-PD-L1 dox had the most significant therapeutic effect in extending the lifetime.

In the survival study, luciferase-labeled ^{luc}CT-26 cancer cells were observed using a real-time bioluminescence imaging system once a week to assess cancer progression in the surviving orthotopic colon cancer-bearing mice. The results showed that both eLipo anti-PD-L1 and eLipo anti-PD-L1 dox evidently inhibited the progression of cancer. Besides, other treatments (anti-PD-L1, Lipo anti-PD-L1, eLipo anti-PD-L1, dox, Lipo dox, eLipo dox) inhibited the progression of cancer in somewhat different degrees as well. In contrast, the progression of cancer in PBS group was very quick, showing the fast spread of cancer cell fluorescence signal (Fig. 7h).

CT-26 cancer has been reported as pMMR colon cancer, whereas MC-38 cancer has been ascribed to dMMR colon cancer^{42–45}. Accordingly, the efficacy was further validated in dMMR colon cancer models in both female and male mice. After treatment with various formulations (PBS pH 7.4, anti-PD-L1, Lipo anti-PD-L1, eLipo anti-PD-L1, dox, Lipo dox, eLipo dox, Lipo anti-PD-L1 dox, and eLipo anti-PD-L1 dox; Fig. 8a; Fig. 9a), tumor volume was measured (Fig. 8b–k; Fig. 9b–k), survival curve was evaluated (Fig. 8l; Fig. 9l), and the body weight was monitored (Fig. 8m; Fig. 9m). The results demonstrated that eLipo anti-PD-L1 significantly inhibited tumor growth and extended the lifetime, while eLipo anti-PD-L1 dox further enhanced the efficacy. In addition, both eLipo anti-PD-L1 and eLipo anti-PD-L1 dox did not cause significant change of body weight, indicating a preliminary safety in mice.

Accordingly, the design and immune activation of protease-cleavable liposome could be illustrated as the following two aspects: (a) The protease-cleavable PD-L1 antibody liposome (eLipo anti-PD-L1) was constructed by tandemly linked anti-PD-L1 with blood long circulation material (PEG₂₀₀₀), legumain-specific cleavage fragment (AAN), and cancer homing peptide (CHP) on the membrane of regular liposome, while doxorubicin was encapsulated into the inner vesicle of eLipo anti-PD-L1. The liposome was cleaved by legumain into two parts in colon cancer site, including the pegylated anti-PD-L1 moiety and the cancer homing liposome moiety (loaded with doxorubicin). (b) Immunotherapy response was activated by the cleaved moiety of pegylated anti-PD-L1 through blocking the binding between PD1 on CD8⁺ T cell with PD-L1 on colon cancer cell, thereby activating the immune killing effect of CD8⁺ T cell through releasing cytokines (IFN- γ , TNF- α). Furthermore, the other cleaved moiety of cancer-homing Dox liposome acts chemotherapy through targeting binding of CHP peptide with neuropilin-1 receptor on cancer cell, and then playing a dual-killing effect (Fig. 10).

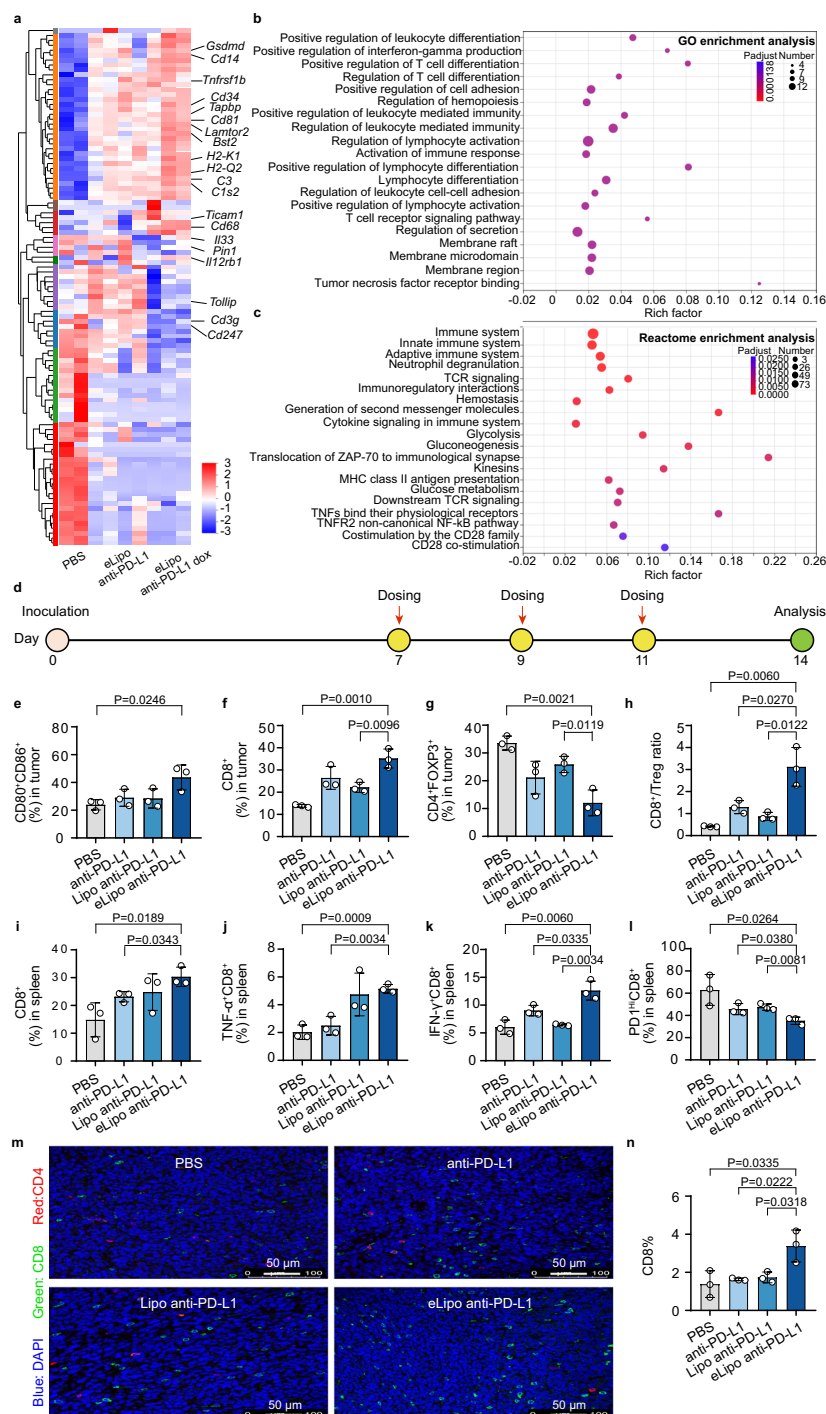


Fig. 6 | Activation mechanism of immune response. **a–c** Activation of immune response ex vivo. The study was performed on the co-culture system of CD8⁺ T cells with colon cancer cells ($n = 3$ independent experiments). CD8⁺ T cells were sorted from spleen lymphocytes of BALB/c mice by fluorescence activated cell sorting (FACS) on a flow cytometer. After treating with various formulations (PBS, eLipo anti-PD-L1 and eLipo anti-PD-L1 dox), total RNA of CD8⁺ T cells were extracted for transcriptome analysis. Hypergeometric distribution operation was used for differential gene enrichment analysis to obtain P value, followed by Benjamini-Hochberg analysis to obtain Padj value. P value < 0.05 , fold change ≥ 1.2 . **a** Heat map. Red, high expression; blue, low expression. **b** GO enrichment. **c** Reactome enrichment. **d** Scheme for activation in vivo. Orthotopic colon cancer-bearing mice were randomly divided into 4 groups ($n = 3$ mice). Various formulations (PBS, anti-PD-L1, Lipo anti-PD-L1 and eLipo anti-PD-L1) were intravenously injected at a dose of 2.3 mg anti-PD-L1/kg at day 7, 9, and 11. Analyses of lymphocytes and cancer masses

were performed by flow cytometry and by CLSM at day 14, respectively.

e–l Activation of immune response in vivo. The study was performed on above orthotopic colon cancer-bearing mice by flow cytometry ($n = 3$ mice). **e** CD80⁺CD86⁺ cells in tumor tissue. **f** CD8⁺ T cells in tumor tissue. **g** CD4⁺FOXP3⁺ T cells in tumor tissue. **h** Ratio of CD8⁺ T cells/Treg cells in tumor tissue. **i** CD8⁺ T cells in spleen. **j** TNF- α T cells in spleen. **k** IFN- γ CD8⁺ cells in spleen. **l** PD1^{hi} CD8⁺ cells in spleen. **m, n** CD8 expression in tumor tissue. CD8 expression in cancer was performed on orthotopic colon cancer-bearing mice ($n = 3$ mice). **m** CLSM observation. Blue channel (DAPI) indicates the nucleus; green channel (Alexa Fluor 488) indicates the expression of CD8; and red channel (Cy3) indicates the expression of CD4. Scale bar, 50 μ m. **n** Quantification. The images were quantified by image J software. Data are shown as the mean \pm SD. Statistical significance (in **e–l, n**) was determined by a two-tailed unpaired t test. Source data are provided as a Source Data file.

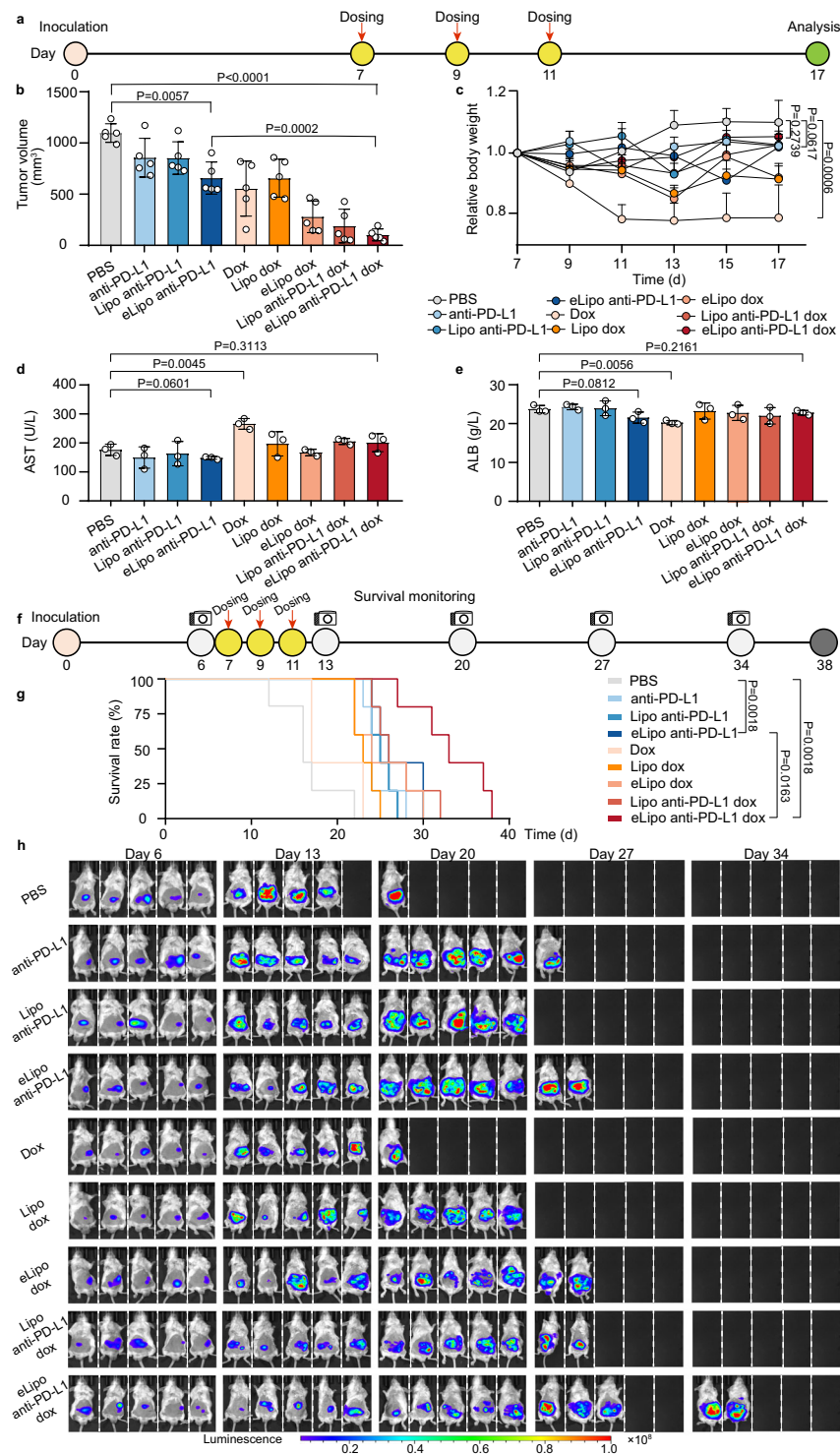


Fig. 7 | Therapeutic efficacy in colon cancer-bearing mice. **a** Scheme for inhibitory effect on cancer growth. Colon cancer-bearing mice were established by orthotopically inoculating 3×10^6 colon cancer CT-26 cells in *BALB/c* mice, and randomly divided into 9 groups. Various formulations (PBS, anti-PD-L1, Lipo anti-PD-L1, eLipo anti-PD-L1, dox, Lipo dox, eLipo dox, Lipo anti-PD-L1 dox, and eLipo anti-PD-L1 dox) were intravenously injected at a dose of 3 mg dox/kg and/or 2.3 mg anti-PD-L1/kg at day 7, 9, and 11. Body weight was recorded every 2 days from day 7 to day 17. Tumor masses and serum samples were collected at day 17. **b** Inhibitory effect on cancer growth. Tumor volume was measured with a vernier caliper at day 17 ($n = 5$ mice). **c** Body weight. Body weight was analyzed by relative body weight (W_t/W_0 ; $n = 5$ mice). **d** AST value. Serum samples were collected at day 17 for measuring aspartate transaminase (AST; $n = 3$ mice). **e** ALB value. Serum samples

were collected at day 17 for measuring albumin (ALB; $n = 3$ mice). **f** Scheme for survival and imaging observation. Colon cancer-bearing mice were established by orthotopically inoculating luciferase-labeled ^{luc}CT-26 cancer cells in *BALB/c* mice. Grouping and dosing strategies were the same as above. **g** Survival curve. Kaplan-Meier survival curves were plotted for colon cancer-bearing mice ($n = 5$ mice). **h** Bioluminescent imaging. Bioluminescence images were captured to observe cancer growth once a week from day 6 to day 34 ($n = 5$ mice). Data are shown as the mean \pm SD. Statistical significance (in **b**) was determined by a one-way ANOVA test, followed by a Turkey multiple comparisons post-test. Statistical significance (in **c**, **d**, **e**) was determined by a two-tailed unpaired *t* test. Survival significance (in **g**) was analyzed by the log-rank test. Source data are provided as a Source Data file.

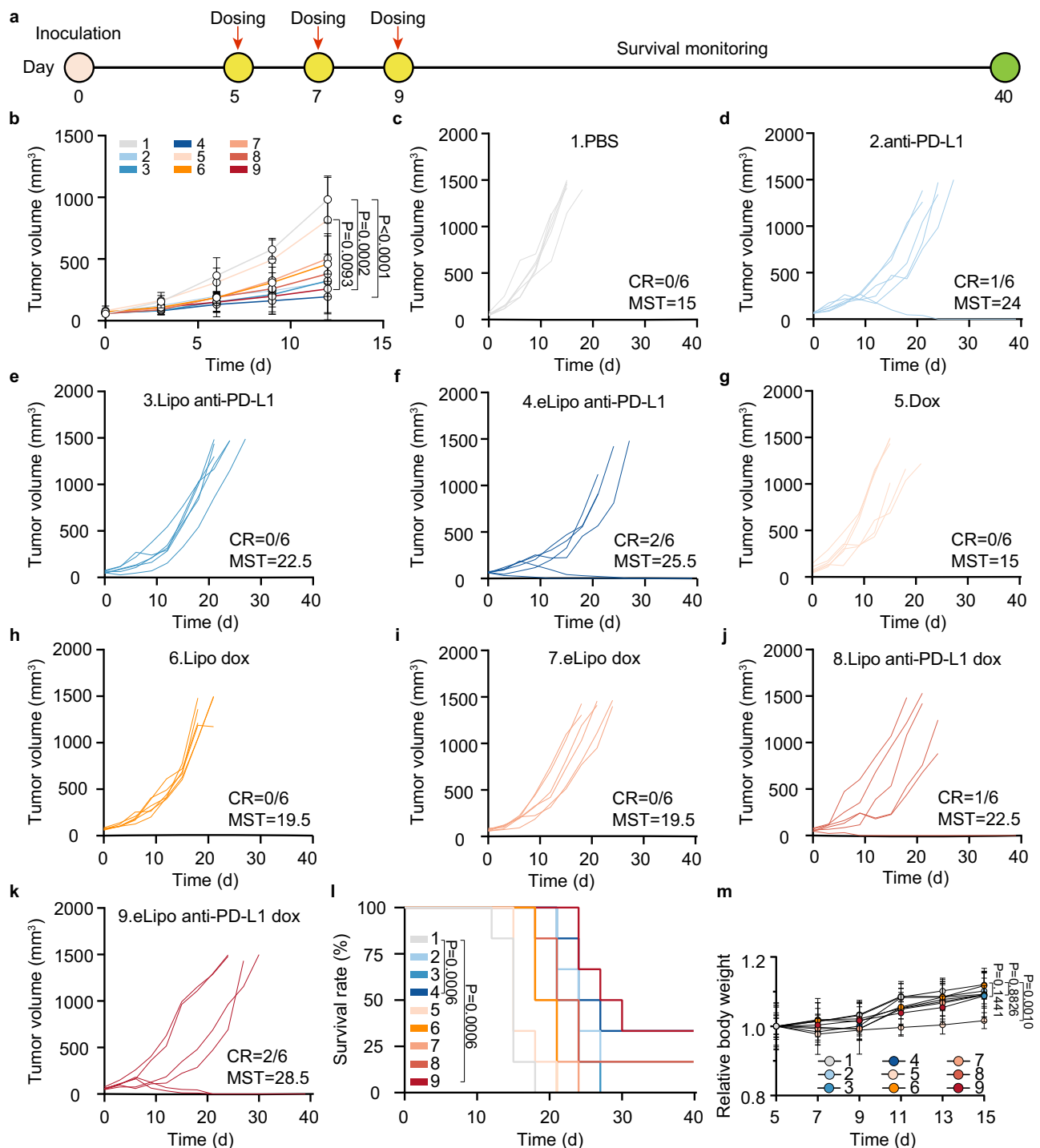


Fig. 8 | Therapeutic efficacy in subcutaneously inoculated colon cancer female mice. **a** Scheme for the inhibitory effect on cancer growth. Colon cancer female mice were established by subcutaneously inoculating 3×10^6 colon cancer MC-38 cells in *C57BL/6* mice, and randomly divided into 9 groups. Various formulations (PBS, anti-PD-L1, Lipo anti-PD-L1, eLipo anti-PD-L1, dox, Lipo dox, eLipo dox, Lipo anti-PD-L1 dox, and eLipo anti-PD-L1 dox) were intravenously injected at a dose of 3 mg dox/kg and/or 2.3 mg anti-PD-L1/kg at day 5, 7, and 9. Tumor volume was measured every 3 days starting from Day 0. Body weight was recorded every 2 days from day 5 to day 15. **b** Inhibitory effect on cancer growth. Tumor volumes were measured with a vernier caliper every 3 days. Results represent the data from day 0 to day 12 ($n = 6$ mice). **c–k** Individual tumor growth profile. Tumor volumes

were measured with a vernier caliper every 3 days. Data were recorded from day 0 until death ($n = 6$ mice). **c** PBS; **d** anti-PD-L1; **e** Lipo anti-PD-L1; **f** eLipo anti-PD-L1; **g** Dox; **h** Lipo dox; **i** eLipo dox; **j** Lipo anti-PD-L1 dox; **k** eLipo anti-PD-L1 dox. CR, complete response; MST, median survival time. **l** Survival curve. Kaplan–Meier survival curve was plotted for the subcutaneously inoculated colon cancer female mice ($n = 6$ mice). **m** Body weight. Body weight of each mouse was analyzed by relative body weight (W_t/W_0 ; $n = 6$ mice). 1, PBS; 2, anti-PD-L1; 3, Lipo anti-PD-L1; 4, eLipo anti-PD-L1; 5, Dox; 6, Lipo dox; 7, eLipo dox; 8, Lipo anti-PD-L1 dox; 9, eLipo anti-PD-L1 dox. Data are shown as the mean \pm SD. Statistical significance (in **b**, **m**) was determined by a two-tailed unpaired *t* test. Survival significance (in **l**) was analyzed by the log-rank test. Source data are provided as a Source Data file.

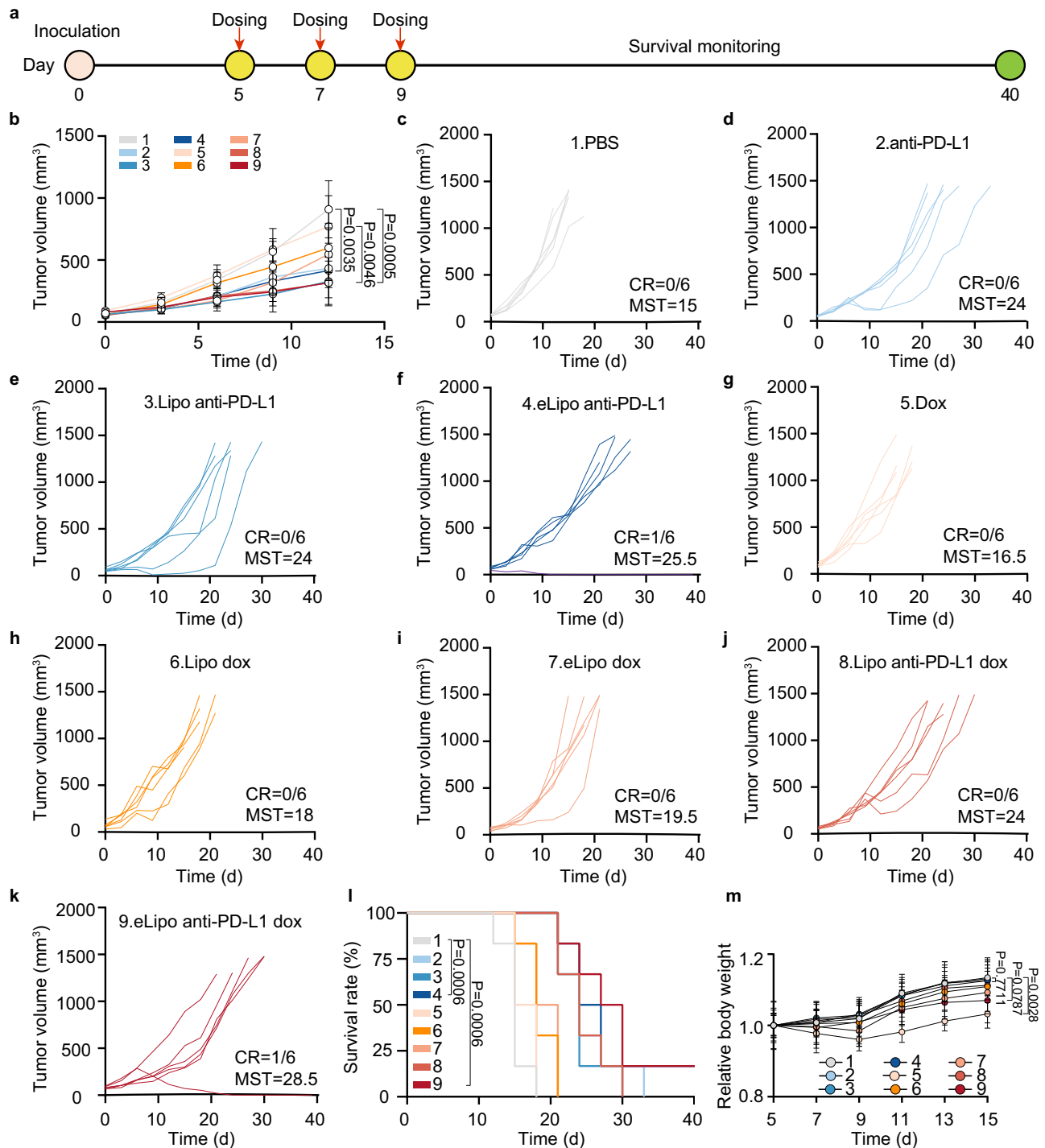


Fig. 9 | Therapeutic efficacy in subcutaneously inoculated colon cancer

male mice. **a** Scheme for the inhibitory effect on cancer growth. Colon cancer male mice were established by subcutaneously inoculating 3×10^6 colon cancer MC-38 cells in *CS7BL/6* mice, and randomly divided into 9 groups. Various formulations (PBS, anti-PD-L1, Lipo anti-PD-L1, eLipo anti-PD-L1, dox, Lipo dox, eLipo dox, Lipo anti-PD-L1 dox, and eLipo anti-PD-L1 dox) were intravenously injected at a dose of 3 mg dox/kg and/or 2.3 mg anti-PD-L1/kg at day 5, 7, and 9. Tumor volume was measured every 3 days starting from Day 0. Body weight was recorded every 2 days from day 5 to day 15. **b** Inhibitory effect on cancer growth. Tumor volumes were measured with a vernier caliper every 3 days. Results represent the data from day 0 to day 12 ($n = 6$ mice). **c–k** Individual tumor growth profile. Tumor volumes were

measured with a vernier caliper every 3 days. Data were recorded from day 0 until death ($n = 6$ mice). **c** PBS; **d** anti-PD-L1; **e** Lipo anti-PD-L1; **f** eLipo anti-PD-L1; **g** Dox; **h** Lipo dox; **i** eLipo dox; **j** Lipo anti-PD-L1 dox; **k** eLipo anti-PD-L1 dox. CR, complete response; MST, median survival time. **l** Survival curve. Kaplan–Meier survival curve was plotted for the subcutaneously inoculated colon cancer male mice ($n = 6$ mice). **m** Body weight. Body weight of each mouse was analyzed by relative body weight (W_t/W_0 ; $n = 6$ mice). 1, PBS; 2, anti-PD-L1; 3, Lipo anti-PD-L1; 4, eLipo anti-PD-L1; 5, Dox; 6, Lipo dox; 7, eLipo dox; 8, Lipo anti-PD-L1 dox; 9, eLipo anti-PD-L1 dox. Data are shown as the mean \pm SD. Statistical significance (in **b**, **m**) was determined by a two-tailed unpaired *t* test. Survival significance (in **l**) was analyzed by the log-rank test. Source data are provided as a Source Data file.

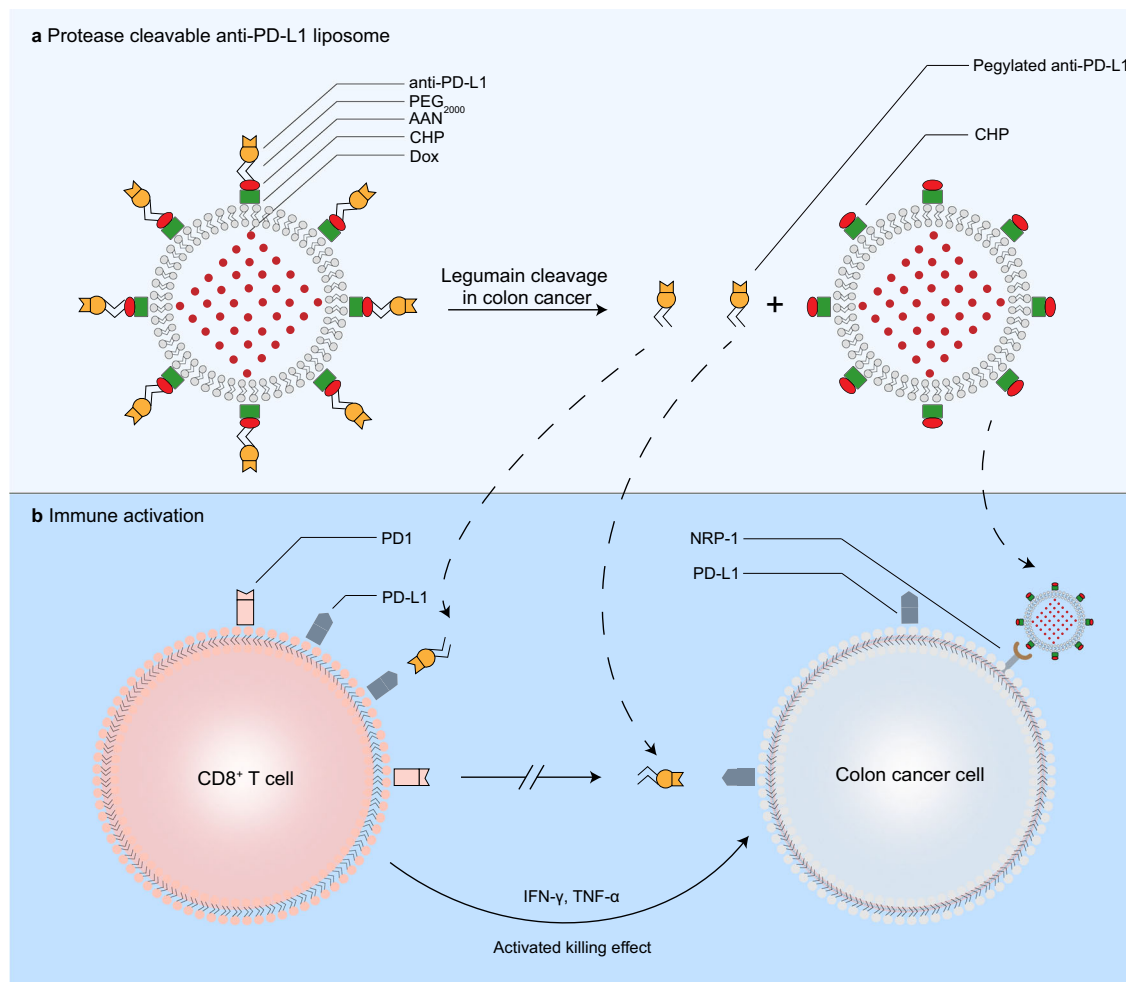


Fig. 10 | Illustration for protease-cleavable checkpoint blockade antibody liposome. **a** Liposome design. The specific protease-cleavable PD-L1 antibody liposome (eLipo anti-PD-L1) is designed for boosting immune checkpoint blockade therapy of colon cancer by synthesizing a functional liposome material with blood long circulation (PEG₂₀₀₀), legumain-specific cleavage (AAN), and cancer homing ability (CHP). Doxorubicin is further encapsulated into the inner vesicle of eLipo anti-PD-L1 for enhancing the immunochemotherapy by co-delivery. The liposome could be cleaved specifically by legumain into two parts in colon cancer site, including the pegylated anti-PD-L1 part and the cancer homing liposome part (enabling co-delivery of doxorubicin). anti-PD-L1, PD-L1 antibody; eLipo anti-PD-L1,

legumain protease-cleavable anti-PD-L1 liposome; PEG₂₀₀₀, polyethylene glycol 2000; AAN, alanine-alanine-asparagine; CHP, cancer homing peptide (cysteine-glycine-asparagine-lysine-arginine-threonine-arginine, CGNKRTR); dox, doxorubicin. **b** Immune activation. The cleaved pegylated anti-PD-L1 part plays an immune checkpoint blockade role by blocking the binding between PD-1 and PD-L1, which exhibited both on CD8⁺ T cell and colon cancer cell. And then cytokines (IFN- γ , TNF- α) were activated to kill cancer cell. In addition to these, the cancer homing liposome part carrying doxorubicin is endocytosed by colon cancer cell through targeting binding of CHP peptide with neuropilin-1 (NRP-1) receptor, playing a dual-killing effect.

Discussion

In today's new major disease treatment strategies, immune checkpoint therapy can be regarded as a powerful transformative treatment strategy, which is marked by the activation of the body's own immunity to correct the disease state. PD-1/PD-L1 therapy is a milestone in cancer treatment, as it is different from other treatment strategies due to its high efficiency and radical treatment in a variety of critical cancer diseases like melanoma, non-small cell lung cancer, renal cell cancer⁷, etc. However, this highly effective strategy has not been able to demonstrate the expected efficacy in many other solid tumors, such as colon cancer. The underlying reason could be strongly associated with the insufficient accumulation of therapeutic immune checkpoint blockade antibody in the tumor site, except for the patients' intrinsic immune exhaustion and immune resistance. Therefore, designing an effective immune antibody delivery vector is critical to the further development of this transformative technology, no less important than reinventing an innovative drug. In this study, we develop a novel protease-cleavable liposome, which can be used as an efficient delivery carrier for immune checkpoint blockade

antibody and anticancer drug as well for immunochemotherapy of colon cancer.

For enriching the immune antibody and/or chemotherapeutic agent into the deep colon cancer site, we design a protease-cleavable liposome as the carrier by taking advantage of the abundant expression of legumain protease in colon cancer. For achieving this intent, the functional liposome material (eLipid-Mal, DSPE-CHP-AAN-K-PEG₂₀₀₀-Mal) is newly synthesized, with blood long circulation (PEG₂₀₀₀, polyethylene glycol 2000), legumain-specific cleavage (AAN, alanine-alanine-asparagine), and cancer homing ability (CHP, cysteine-glycine-asparagine-lysine-arginine-threonine-arginine, CGNKRTR). The synthesized products are successfully identified by physicochemical methods, including NMR, HPLC, and MALDI-TOF mass spectroscopy (Fig. 1).

The designed liposome can be cleaved by protease into two parts, including a pegylated anti-PD-L1 part and a cancer homing peptide conjugated liposome part (enabling the simultaneous co-delivery of doxorubicin). The cleavability of the liposome is achieved by rational synthesizing a unique functional material that contains a

cleavable AAN tripeptide fragment. It is due to the fact that the acyl bond of asparagine in AAN can be specifically cleaved by legumain protease^{46,47}. For preparing the protease-cleavable liposome, the mole ratio of eLipid-Mal/anti-PD-L1 is optimized by evaluating anti-PD-L1 coupling efficiency and anti-PD-L1 amount, respectively. The results show that there is a reverse V-shaped trend between eLipid-Mal/anti-PD-L1 ratio and the coupling amount of anti-PD-L1. The likely reason is that, with the increase of anti-PD-L1 molar concentration, the -Mal binding sites are occupied gradually. Nevertheless, the number of -Mal groups on liposome is fixed, once the binding between -Mal group and anti-PD-L1 reaches saturation, the addition of excessive anti-PD-L1 will reversely affect the coupling efficiency. In addition, other indicators are also involved for selecting an optimal engineering procedure, including the nanoparticle size, and zeta potential (Fig. 2).

The functional verification of the protease-cleavable liposome has been performed from several aspects. Firstly, legumain and PD-L1 are evidenced in high expression in the colon cancer site and on the cancer cells, respectively. These results provide the premise for the protease cleavage and for acting immune checkpoint therapy of the protease-cleavable liposome. Secondly, the protease cleavage activity is verified by the fluorescent substrate. In addition, it is demonstrated that the cleaved pegylated anti-PD-L1 still plays a highly efficient immune checkpoint blockade effect, and the cleaved liposome part enables a targeting endocytosis by colon cancer cells (Fig. 3). For evaluating the potential applicability of protease-cleavable liposome, the expressions of PD-L1 and legumain are confirmed in human colorectal tissues with the microarray consisting of 50 colorectal cancer tissue specimens (18 females and 32 males) and their corresponding cancer adjacent tissue specimens. The results indicate that both PD-L1 and legumain are rich expressed in colorectal cancer tissue at different clinical stages (stage I to IV), suggesting a premise for the protease cleavage and for enhancing immune checkpoint blockade therapy of colorectal cancer (Fig. 4). Thirdly, the targeting distribution is demonstrated by a dual-probe fluorescence imaging in the orthotopic colon cancer-bearing mice, and deep penetrating ability is confirmed in the colon cancer spheroids (Fig. 5).

The targeting effect of the liposome can be explained by one or multiple reinforced effect of the following factors, consisting of blood long circulation role, enhanced permeability retention (EPR) effect, CHP peptide, and anti-PD-L1 mediated targeting. The blood long circulation role of the liposome is achieved by modification of PEG₂₀₀₀ polymer, which is able to evade the rapid clearance of PD-L1 antibody by the mononuclear phagocyte system (MPS) in the blood circulation^{24,25}, and such a prolonged blood exposure is able to enhance the accumulation of the liposome in tumor tissue by a passive diffusion and then by EPR effect^{24,48,49}. Besides, it is reported that cancer homing peptide (CHP) is a substrate of neuropilin-1 (NRP-1) receptor, a transmembrane protein expressed on the surface of cancers^{41,50}, and hence, the modified CHP peptide on the liposome can specifically bind with NRP-1 receptor⁵¹, mediating the targeting endocytosis of the liposome by cancer cell. In addition, anti-PD-L1 modification also contributes to the targeting accumulation of the liposome before cleavage, as anti-PD-L1 is also able to specifically bind with PD-L1 of colon cancer cells^{52,53}.

The activation mechanism of immune response has been studied from two aspects: gene alteration and activation of CD8⁺ T cells. Firstly, the protease-cleavable anti-PD-L1 liposome results in a substantial gene alteration in CD8⁺ T cells. The differential genes are involved in promoting interferon-gamma production, enhancing T cell differentiation, activating immune response, regulating T cell receptor signaling pathway, and increasing tumor necrosis factor receptor binding. The relevant signaling pathways were involved in the promotion, including innate immune system, adaptive immune system, T cell receptor signaling pathway, cytokine signaling immune system,

MHC class II antigen presentation, and CD28 co-stimulation. Secondly, as the result of gene regulation, the protease-cleavable anti-PD-L1 liposome remarkably increases the recruitment of cytotoxic T lymphocytes (CTLs, CD8⁺ T cells), promotes the productions of TNF- α and IFN- γ , while restores the exhausted T lymphocytes (PD1^{hi}CD8⁺ T lymphocytes (Fig. 6). As the consequence of activation, both protease-cleavable anti-PD-L1 liposome (eLipo anti-PD-L1) and protease-cleavable anti-PD-L1 plus doxorubicin liposome (eLipo anti-PD-L1 dox) remarkably enhance the therapeutic efficacy in the orthotopic pMMR colon cancer-bearing mice (Fig. 7), respectively. For further verifying the therapeutic efficacy of protease-cleavable liposome in dMMR colon cancer-bearing mice, a subcutaneous colon cancer-bearing mouse model is established with colon cancer MC-38 cells. Besides, both female (Fig. 8) and male (Fig. 9) mice are included for assessing the influence of sex on therapeutic efficacy. The results demonstrate that the protease-cleavable liposome exhibits the most significant anti-cancer efficacy as compared to the controls, and mouse sex does not affect these results.

In sum, we successfully engineer a protease-cleavable checkpoint blockade antibody liposome (eLipo anti-PD-L1) by rationally designing a functional liposome material with blood long circulation, legumain-specific cleavage, and cancer homing ability. The results demonstrate that the liposome is able to be cleaved specifically by legumain into two parts in the colon cancer environment, including the pegylated anti-PD-L1 part and the cancer homing liposome part (enabling co-delivery of doxorubicin). The rich expressions of PD-L1 and legumain are verified in the colon cancer-bearing mice and human colorectal cancer tissues (18 females and 32 males) as well, indicating a potential clinical applicability of protease-cleavable liposome. The protease-cleavable liposome exhibits a targeting distribution in colon cancer tissue, a deep penetrating ability in colon cancer spheroid, legumain-responsive cleavage characteristics, cancer cell targeting endocytosis, and immune activating effects. eLipo anti-PD-L1 alone demonstrates a remarkable therapeutic efficacy, and the co-delivery of doxorubicin (eLipo anti-PD-L1 dox) further enhances the efficacy in the colon cancer-bearing mice and mouse sex does not affect these results. Accordingly, as a versatile immune checkpoint blockade antibody delivery platform, the protease-cleavable liposome has the potential for broad uses by co-delivering chemotherapeutic agents for the treatment of various immune inefficient solid cancers. In conclusion, this study develops a novel protease-cleavable liposome, which can be used as not only an efficient delivery carrier for immune checkpoint blockade therapy but also a multiple platform for immunochemotherapy to treat colon cancer.

Methods

Materials

1,2-Distearoyl-sn-glycero-3-phosphoethanolamine (DSPE) was synthesized by Xi'an Ruixi Biological Technology (Xi'an, China). Cysteine-glycine-asparagine-lysine-arginine-threonine-arginine (CGNKRTR, CHP) was synthesized by Top-Peptide (Shanghai, China). 1,2-Distearoyl-sn-glycero-3-phosphoethanolamine polyethylene glycol 2000 maleimide (DSPE-PEG₂₀₀₀-Mal) was purchased from NOF Corporation (Tokyo, Japan). Egg phosphatidylcholine was purchased from Avanti Polar Lipids (Alabaster, USA). Cholesterol was purchased from J&K Scientific (Beijing, China). Doxorubicin hydrochloride (#MB1087-2) was purchased from Dalian Meilun Biotech (Dalian, China). Recombinant mouse PD-L1 (C-Fc, #CJ89; PD-L1 protein), recombinant mouse neuropilin-1 (C-6His, #C11R; NRP-1), recombinant mouse IL-2 (#CK24), and recombinant mouse IL-7 (C-6His, #CC73) were purchased from Novoprotein (Shanghai, China). Recombinant mouse legumain protein (His Tag, #50051-M07H) was purchased from Sino Biological (Beijing, China). InVivoMab anti-mouse PD-L1 (B7-H1) (clone: 10 F.9G2; anti-PD-L1) was purchased from BioXcell (Beijing local agent, USA). RR-11a analog (#HY-112205A) was purchased from MedChemExpress (MCE,

Beijing local agent, USA). Purified anti-mouse CD3 ϵ (#100339), purified anti-mouse CD28 (#102115), FITC anti-mouse CD11c (#117306), PE anti-mouse CD80 (#104707), PE-Cy 7 anti-mouse CD86 (#105013), PE-Cy7 anti-mouse CD45 (#103113), FITC anti-mouse CD3 ϵ (#100305), PerCP/Cyanine5.5 anti-mouse CD4 (#100433), Brilliant Violet 421™ anti-mouse CD8a (#100753), PE anti-mouse FOXP3 (#126404), PE anti-mouse IFN- γ (#505807), APC anti-mouse TNF- α (#506307), APC anti-mouse CD279 (PD1, #135209), Zombie Aqua™ fixable viability kit (#423101), and APC anti-mouse CD274 (PD-L1, #124311) were purchased from BioLegend (Beijing local agent, USA). APC anti-mouse CD304 (Neuropilin-1, #3DS304M) was purchased from eBiosciences (Beijing local agent, UK). HRP goat anti-rat IgG (#AS028) was purchased from Abclonal (Wuhan, China). 1,1-Dioctadecyl-3,3,3-tetramethylindotricarbocyanine iodide (DiR, #D9320), DNase (#D8071), hyaluronidase (#H8030), collagenase IV (#C8160), and D-luciferin potassium salt (#D9390) were purchased from Solarbio (Beijing, China). 2-Morpholinoethanesulphonic acid (MES, #M22274) was purchased from Harveybio (Beijing, China). HBS-EP (0.01 M HEPES, 0.15 M NaCl, 3 mM EDTA, 0.005% v/v surfactant P20; pH 7.4) was purchased from GE Healthcare (Boston, USA).

Cells and animals

Colon cancer CT-26 cells (#1101MOU-PUMC000275), MC-38 cells (#1101MOU-PUMC000523), and Caco-2 cells (1101HUM-PUMC000100) were purchased from the Institute of Basic Medical Sciences, Chinese Academy of Medical Sciences (Beijing, China). Colon cancer CMT-93 cells (#ZQ1083) were purchased from Zhong Qiao Xin Zhou Biotechnology Co., Ltd (Shanghai, China). Luciferase labeled colon cancer ^{luc}CT-26 cells (#FH1129) were purchased from FuHeng Cell Center (Shanghai, China). Both colon cancer CT-26 cells and luciferase-labeled ^{luc}CT-26 colon cancer cells were cultured at 37°C under 5% CO₂ in Roswell Park Memorial Institute (RPMI) 1640 medium (Macgene, China) supplemented with 10% fetal bovine serum (FBS; PAN, Germany), 100 U/mL penicillin, and 100 μ g/mL streptomycin (Macgene, China). Besides, MC-38 cells, CMT-93 cells, and Caco-2 cells were cultured at 37°C under 5% CO₂ in Dulbecco's modified Eagle's medium (DMEM, Macgene, China) supplemented with 10% fetal bovine serum, 100 U/mL penicillin, and 100 μ g/mL streptomycin.

BALB/c mice (6–8 weeks old, 18–20 g, male), C57BL/6 mice (6–8 weeks old, 18–20 g, male), C57BL/6 mice (6–8 weeks old, 18–20 g, female), and *Sprague-Dawley* rats (250–300 g, male) were purchased from Laboratory Animal Center of Peking University Health Science Center (Beijing, China), and all the animal strains were introduced from the National Rodent Laboratory Animal Resources Center (Beijing, China) and bred by the Laboratory Animal Center of Peking University Health Science Center. The mice were kept in the specific pathogen-free (SPF) level system, with free access to sterile food pellets and water. The standard condition included a 12 h light/dark cycle, a moderate temperature maintained at 25 \pm 2 °C, and an appropriate relative humidity maintained at 50 \pm 20%. All the animal experiments were conducted according to the guidelines of the National Institutes of Animal Care and Use Committee, and approved by the Laboratory Animal Welfare Ethics Sub-Committee of Biomedical Ethics Committee at Peking University (No. LA2021252). For subcutaneously inoculated cancer-bearing animals, mice were euthanized by cervical dislocation to minimize pain and distress when the tumor burden exceeded 1500 mm³. For orthotopically inoculated cancer-bearing animals to observe the survival period after drug administration, tumor size could not be measured directly, while death was an inevitable endpoint so as to provide an objective and unequivocal data point. In this case, animals were observed twice a day to detect signs of impending death, including severe pain, distress, prolonged supine inability to walk, etc., and were euthanized by cervical dislocation in time.

Synthesis and identification of enzyme-cleavable material

The enzyme cleavable material was synthesized by a three-step process. Firstly, DSPE (1 eq.) dissolved in chloroform was reacted with suberic anhydride (1.1 eq.) and triethylamine (2.0 eq.) at 60°C for 1 h to form carboxylic acid-modified DSPE, and then carboxylic acid-modified DSPE (1 eq.) was further reacted with 1-(3-dimethylaminopropyl)-3-ethylcarbodiimide hydrochloride (EDC; 1.5 eq.) and N-hydroxy succinimide (NHS; 1.5 eq.) at 40 °C for 3 h to obtain DSPE-NHS. Secondly, functional peptide (CHP-AAN-K) was synthesized using cysteine-glycine-asparagine-lysine-arginine-threonine-arginine (CGNKRTR; a cancer homing peptide, CHP), alanine-alanine-asparagine (AAN; a cleavable peptide by legumain at N site), and lysine (K) through a solid-phase synthesis, and then reacted with a linear heterobifunctional polyethylene glycol (COOH-PEG₂₀₀₀-Mal) to form CHP-AAN-K-PEG₂₀₀₀-Mal. Finally, DSPE-NHS was covalently linked with CHP-AAN-K-PEG₂₀₀₀-Mal to form eLipid-Mal (DSPE-CHP-AAN-K-PEG₂₀₀₀-Mal).

The synthesized product of DSPE-NHS was identified by nuclear magnetic resonance (¹H NMR, Bruker, 600 Hz, CDCl₃) for identifying its structure. The functional peptide (CHP-AAN-K) product was identified by liquid chromatography-mass spectrometry (LC-MS), and the purity of CHP-AAN-K was measured by high-performance liquid chromatography with ultraviolet detection (HPLC-UV). The molecular weight distribution of CHP-AAN-K-PEG₂₀₀₀-Mal and eLipid-Mal were characterized by matrix-assisted laser desorption/ionization time-of-flight (MALDI-TOF) mass spectrometry (AB SCIEX, Singapore), respectively. The molecular weight range was estimated by the mass/charge (m/z) ratio.

Preparation and characterization of protease-cleavable liposome

Egg phosphatidylcholine, cholesterol, and eLipid-Mal (DSPE-CHP-AAN-K-PEG₂₀₀₀-Mal) were used as the membrane materials (60: 36: 4, mol/mol), and the blank liposome (blank eLipo) was prepared by film dispersion, followed by membrane extrusion. Anti-PD-L1 was then conjugated onto the -Mal group of eLipid-Mal under 4°C to prepare the protease-cleavable anti-PD-L1 liposome (eLipo anti-PD-L1). Besides, doxorubicin was encapsulated into the blank eLipo using ammonium sulfate gradient method and then conjugated with anti-PD-L1 to prepare the protease-cleavable anti-PD-L1 plus dox liposome (eLipo anti-PD-L1 dox). The control liposomes were similarly prepared, including blank Lipo, blank eLipo, Lipo dox, eLipo dox, Lipo anti-PD-L1, and Lipo anti-PD-L1 dox. The membrane materials used in the control liposomes were slightly different through adding or excluding a different material for a specific control purpose.

The size and zeta potential values of various formulations were characterized using dynamic light scattering (DLS; Malvern Panalytical, UK). The morphology of various formulations was observed by transmission electron microscopy (TEM; JEM-2100, Japan), and atomic force microscopy (AFM) (Dimension Icon, Bruker, Germany), respectively.

The encapsulation efficiency of doxorubicin in the liposome was measured by decomposing the liposome in methanol and then assayed by fluorescence spectrometry (Cary Eclipse, Agilent, USA; Ex = 488 nm, Em = 585 nm). The loading efficiency of anti-PD-L1 on the liposome was measured by quantifying anti-PD-L1 amount using the enzyme linked immunosorbent assay (ELISA) kit.

The conjugation of anti-PD-L1 with the liposome was verified by Western blot assay. Briefly, anti-PD-L1, Lipo anti-PD-L1, and eLipo anti-PD-L1 were quantified using a bicinchoninic acid (BCA) protein assay kit according to the manufacturer's instruction, and further separated by sodium dodecyl sulfate-polyacrylamide gel electrophoresis (SDS-PAGE). The separated proteins were transferred onto polyvinylidene fluoride (PVDF) membranes (Merck Millipore, Germany). The blots on PVDF membranes were blocked with 5% bovine serum albumin (BSA) in TBS-T (Tris-buffered saline with Tween 20) solution, and further

incubated with horseradish peroxidase (HRP)-conjugated secondary antibodies at 25 °C for 1 h. Finally, the blots were observed by a Mini-Chemi610 imaging system (Sage Creation, China).

Doxorubicin release profile of eLipo anti-PD-L1 dox

The in vitro release of doxorubicin from the eLipo anti-PD-L1 dox was measured by a dialysis method. Two phosphate buffer solutions with different pH values (PBS pH 5.5, and PBS pH 7.4) were used as drug release media. Briefly, 1 mL eLipo anti-PD-L1 dox suspension was sealed in the dialysis bag (MWCO 3500 Da), and then immersed in 30 mL release medium. The dialysis apparatus was gently shaken at 100 revolutions per minute (rpm) at 37 °C. At a fixed time-point, 0.5 mL release medium was sampled, followed by adding an equal volume of fresh release medium. The released amount of doxorubicin was measured by fluorescence spectrometry (Agilent Cary Eclipse, USA; Ex = 488 nm, Em = 585 nm).

Colon cancer-bearing mouse models

The orthotopic colon cancer-bearing mouse models were established by abdominal laparotomy inoculation. Briefly, *BALB/C* mice (6–8 week) were prepared for abdominal laparotomy after removing hair and disinfecting the mice abdomen. Colon cancer CT-26 cells and luciferase labeled colon cancer ^{luc}CT-26 cells were prepared into single cell suspensions, respectively. Single cell suspension (3×10^6) was gently injected into specific colon location, in which blood vessels were dense and blood flow was abundant. After inoculation at day 7, the orthotopic colon cancer model was established successfully, and confirmed by imaging the luciferase labeled cancer cells using a biofluorescence LivingImage system (IVIS Spectrum, PerkinElmer, USA).

Besides, a colon cancer mouse model was also established by subcutaneous injection of 1×10^6 colon cancer CT-26 cells into the left flank of *BALB/c* mice. In addition, a colon cancer mouse model was established by subcutaneous injection of 3×10^6 colon cancer MC-38 cells into the left flank of *C57BL/6* mice.

Expressions of legumain, PD-L1 and NRP-1

The expressions of legumain enzyme and PD-L1 protein were confirmed in the tumor site of the orthotopic colon cancer-bearing *BALB/c* mice model, and the subcutaneous colon cancer-bearing mice model, respectively (6 mice for each group). Briefly, tumor masses were collected from the cancer-bearing mice, fixed with 4% paraformaldehyde, embedded in paraffin, and sectioned, followed by immunofluorescence imaging using confocal laser scanning microscopy (CLSM; TCS-SP8, Leica, Germany). In addition, the expressions of PD-L1 protein and NRP-1 receptor were evaluated on the colon cancer CT-26 cells, MC-38 cells, CMT-93 cells, and Caco-2 cells. Briefly, colon cancer CT-26 cells, MC-38 cells, CMT-93 cells, and Caco-2 cells were stained with APC anti-mouse CD274 and APC anti-mouse CD304 according to the manufacturer's instruction, and measured by a flow cytometry (FACS Calibur™, BD, USA).

Legumain specific cleavage capability

Legumain specific cleavage ability was indicated by a fluorogenic peptide substrate (CBZ-AAN-AMC). Briefly, recombinant mouse legumain protein or cancer tissue homogenate was diluted in the buffer (0.1 M NaOAc, 0.1 M NaCl, pH 4.5) and incubated at 37 °C for 4 h as the activated legumain solution (*solution A*). The substrate (CBZ-AAN-AMC) and the legumain-specific cleavage inhibitor (RR-11a) were dissolved in dimethyl sulfoxide (DMSO), and then diluted with the buffer (50 mM MES, 250 mM NaCl, pH 5.5) as the substrate solution (*solution B*) and the inhibitor solution (*solution C*), respectively. The *solution A* and the *solution B* were mixed in the 96-well culture plate (containing 2 ng/μL legumain and 200 μM CBZ-AAN-AMC), incubated at 37 °C for 2 h, and measured by the fluorescence

microplate reader (Synergy Neo2, BioTek, USA; Ex = 353 nm, Em = 420–500 nm). Besides, the *solution A*, the *solution B* and the *solution C* were mixed in the 96-well culture plate (containing 2 ng/μL legumain, 200 μM CBZ-AAN-AMC, and 2 μM RR-11a), and the same measured by the fluorescence microplate reader. In addition, the *solution B* and the buffer (50 mM MES, 250 mM NaCl, pH 5.5) were mixed as the blank control. The fluorescence values were used to indicate legumain specific cleavage ability on the asparagine site of AAN segment.

Specific binding of anti-PD-L1 with PD-L1, and CHP with NRP-1

The specific binding ability of anti-PD-L1 with PD-L1 was evaluated by surface plasmon resonance (SPR) assay. Briefly, recombinant mouse PD-L1 (20 μg/mL) was dissolved in acetate buffer (pH 4.5) and then immobilized on a CM5 sensor chip of the SPR system (Biacore T200, GE Healthcare, USA) using the amine coupling kit. Afterwards, anti-PD-L1 (0.20–3.0 nM) or eLipo anti-PD-L1 (0.50–8.0 μM anti-PD-L1) sample was injected into SPR system for analysis. The flow rate was 30 μL/min, the assay temperature was set at 25 °C, and the running buffer was HBS-EP solution (0.01 M HEPES, 0.15 M NaCl, 3 mM EDTA, 0.005% v/v surfactant P20; pH 7.4). The chip was equilibrated with the running buffer for 10 s before the next injection. The data were analyzed with the Biacore evaluation software (T200 Version 1.0, GE Healthcare, UK) by curve fitting using a 1:1 binding model.

The specific binding ability of CHP with NRP-1 was similarly evaluated by SPR assay. Briefly, the chip was firstly regenerated for 30 s with NaOH (10 mM). The recombinant mouse neuropilin-1 (NRP-1, 50 μg/mL) was dissolved in acetate buffer solution (pH 4.0), and then immobilized on a CM5 sensor chip of the SPR system using the amine coupling kit. Free CHP (1.6–25.0 μM), eLipo (1.0–30.0 pM CHP), and eLipo (1.6–50.0 pM CHP) plus legumain (2 ng/mL) sample was injected into the SPR system. Other analysis conditions were the same as above.

Expressions of PD-L1 and legumain in human colorectal cancer specimens

Human colon cancer tissue microarray (Code No.: D100Co01) was obtained from Zhongke Guanghai Intelligent Biotechnology Co., Ltd (Xi'an, China). Briefly, the microarray was from 18 females and 32 males for a total of 50 patients with colon cancer tissues (from stage I to stage IV) and their corresponding adjacent tissues. The age of the patients ranged from 32 to 83 years. Immunofluorescence staining of the microarray was performed with anti-PD-L1 antibody (28076-1-AP, Proteintech, China) and anti-legumain antibody (sc-133234, Santa Cruz Biotechnology, USA). The quantification of the images was performed by professional pathological diagnosis. The experiment was approved by Peking University Institutional Review Board (IRB 00001052-24172).

Distribution in vivo and ex vivo

The targeting distribution of the enzyme cleavable liposome (eLipo anti-PD-L1 dox) was separately evaluated on the orthotopic colon cancer-bearing mice from two aspects, including the cleaved pegylated anti-PD-L1 part and the cleaved liposome part, considering its cleavage in vivo. For achieving this purpose, the enzyme cleavable liposome was dual-labeled by two fluorescence probes, namely, sulfo-cyanine 5.5 N-hydroxy succinimide ester (Cy5.5), and 1,1-dioctadecyl-3,3,3,3-tetramethylindotricarbocyanine iodide (DiR). To understand the distribution of the pegylated anti-PD-L1 part, Cy5.5 was chemically conjugated with the amino group of anti-PD-L1, enabling Cy5.5 to indicate the distribution of pegylated anti-PD-L1. To observe the distribution of liposome part, DiR was encapsulated into the vesicle of liposome, allowing DiR to indicate the distribution of liposome part.

On the one hand, the orthotopic colon cancer-bearing *BALB/c* mice were randomly divided into 5 groups (3 mice for each group), and

various formulations (PBS pH 7.4, Cy5.5, Cy5.5@anti-PD-L1, Cy5.5DiR@Lipo anti-PD-L1, and Cy5.5DiR@eLipo anti-PD-L1) were separately injected into the mice via tail vein for observing the distribution of pegylated anti-PD-L1, followed by imaging the fluorescence of Cy5.5 at a fixed time-point (2, 4, 8, 12, 24, 48 h) by a LivingImage system (IVIS Spectrum, PerkinElmer, USA; Ex = 680 nm, Em = 710 nm).

On the other hand, the orthotopic colon cancer-bearing *BALB/c* mice were randomly divided into 6 groups (3 mice for each group), and various formulations (PBS pH 7.4, DiR, Lipo DiR, eLipo DiR, Cy5.5DiR@Lipo anti-PD-L1, and Cy5.5DiR@eLipo anti-PD-L1) were separately injected into the mice via tail vein for observing the distribution of liposome part, followed by imaging the fluorescence of DiR at a fixed time-point (2, 4, 8, 12, 24, 48 h) by a LivingImage system (IVIS Spectrum, PerkinElmer, USA; Ex = 750 nm, Em = 780 nm).

Besides, above mice were euthanized at 48 h, and the main organs (heart, liver, spleen, lung, and kidney) and tumor tissues were ex vivo imaged by the same system at the corresponding condition. In addition, the fluorescence intensity in tumor tissues was quantified by Living Image software (Caliper life science, USA).

Pharmacokinetic study

To study the pharmacokinetic behavior of eLipo anti-PD-L1 dox, doxorubicin hydrochloride (dox 3 mg/kg) and eLipo anti-PD-L1 dox (dox 3 mg/kg) were administrated to *Sprague-Dawley* rats via tail vein injection, respectively (3 rats for each group, 2 groups in total). The blood specimens were sampled at the fixed time-points (0, 0.25, 0.5, 0.75, 1, 2, 4, 8, 12, 24, 48 h), and placed in heparin sodium anticoagulated tubes. The plasma samples were obtained by centrifugation at 10,000 *g* for 15 min, and stored at -20 °C until HPLC-MS/MS analysis. The HPLC-MS/MS analysis was performed on a Thermo Fisher Scientific Ultimate 3000 HPLC system (San Jose, USA) coupled with an AB SCIEX 4000 QTRAP mass spectrometer (Foster City, USA) equipped with an electrospray ionization (ESI) source system. The chromatographic separation was carried out on a Waters Acquity BEH C18 column (50 mm × 2.1 mm, 1.7 μm, Agilent Technologies, CA, USA). Mobile phase A was the aqueous phase of 0.1 % formic acid, and mobile phase B was the organic phase of acetonitrile. The mobile phase was delivered at a flow rate of 0.3 mL/min in the following gradient: 0-0.5 min 90-30% A, 0.5-1.0 min 30-0% A, 1.0-3.0 min 0% A, 3.0-3.1 min 0-90% A, 3.1-5.0 min 90% A. For mass spectrometry, ESI positive mode was used and multiple reaction monitoring (MRM) parameters are listed in Supplementary Table 2. Detection parameters were as follows: curtain gas was 15 psi; collision gas was 8 psi; ion spray voltage was 5500 V; temperature was 550 °C; ion source gas 1 and gas 2 were 55 psi and 55 psi, respectively. The HPLC-MS/MS were controlled by Chromeleon chromatography data system software (Thermo Fisher Scientific Inc., San Jose, USA) and Analyst software (Applied Biosystems Inc., Foster City, USA). The pharmacokinetic parameters of doxorubicin were calculated with two-compartmental model (DAS 2.0 software).

Deep penetration in colon cancer spheroids in vitro

For establishing the cancer spheroids, colon cancer CT-26 cells (1×10^6) were seeded into integrated biomimetic array chip (IBAC S1-96, Beijing Daxiang Biotech, China) which was previously coated with rat tail tendon type I collagen (1 mg/mL). After 72 h incubation at 37 °C under 5% CO₂, colon cancer spheroids were clearly observed by fluorescence microscopy, indicating a successful establishment of colon cancer spheroids. Various formulations (Cy5.5, Cy5.5@anti-PD-L1, Cy5.5DiR@Lipo anti-PD-L1, and Cy5.5DiR@eLipo anti-PD-L1) were applied to the colon cancer spheroids, and further incubated at 37 °C under 5% CO₂ for 3 h, and imaged by confocal laser scanning microscopy (TCS-SP8 DIVE, Leica, Germany; 10× objective lens, and 647 nm

diode laser), respectively. The laser intensity and detector gain settings were maintained the same across all image acquisitions. The fluorescence intensity was evaluated by the LAS X Life Science microscopy software (Leica, Germany).

Uptake by colon cancer cell in vitro

Colon cancer CT-26 cells (1×10^4), MC-38 cells (1×10^4), CMT-93 cells (5×10^3), and Caco-2 cells (1×10^4) were cultured in 96-well plate at 37 °C under 5% CO₂ overnight. When the cell confluence reached 80%, pre-activated legumain (2 ng/mL) was added and cultured with the cells for 4 h. Various formulations (PBS pH 7.4, dox, Lipo dox, eLipo dox, Lipo anti-PD-L1 dox, and eLipo anti-PD-L1 dox; 1 μg/mL doxorubicin) were applied to the cancer cells, and further incubated at 37 °C under 5% CO₂ for 3 h, and measured by the operetta CLS high content imaging system equipped with the Harmony analysis software (PerkinElmer, USA), respectively. The cellular uptake of the formulation was indicated by the fluorescence of doxorubicin, while cell nucleus was indicated by the fluorescence of Hoechst 33342 dye. During the imaging process, the cells were maintained in an environmental chamber at 37 °C under 5% CO₂, and imaged with a 20× objective lens.

Fluorescence resonance energy transfer assay

Colon cancer CT-26 cells and T cells were co-cultured, and incubated with anti-PD-L1 under 5% CO₂ at 37 °C for 5 h. Then the cells were incubated with primary PD-L1 antibodies (# 66248-1-Ig, proteintech, Beijing local agent) overnight at 4 °C, stained with secondary antibodies goat anti mouse IgG Alexa Fluor 488 (# ZF-0512, ZSGB-BIO, China) and goat anti rat IgG Alexa fluor 594 (#bs-0293G-AF594, Bioss, China) for 2 h, respectively, and finally stained with DAPI for 30 min. The FRET assay was further performed on colon cancer MC-38 cells, CMT-93 cells, and Caco-2 cells when the cell confluence reached 80%, following the same procedure as above. Images were captured by confocal laser scanning microscopy.

Transcriptome analysis

CD8⁺ T cells were sorted from spleen lymphocytes of *BALB/c* mice by the fluorescence activated cell sorting (FACS) on a flow cytometer (FACS Aria II, BD, USA) (Supplementary Fig. 21). The sorted CD8⁺ T cells were then activated by co-culturing with the activating antibodies (1 μg/mL anti-CD3ε antibody, 5 μg/mL anti-CD28 antibody) and the cytokines (50U IL-2, and 50U IL-7) at 37 °C under 5% CO₂ overnight. Afterwards, the activated CD8⁺ T cells were co-cultured with colon cancer CT-26 cells (CD8⁺ T cells: cancer cells = 5:1) at 37 °C under 5% CO₂ for 24 h. Various formulations (PBS pH 7.4, eLipo anti-PD-L1 and eLipo anti-PD-L1 dox) were applied to the co-culture system, and further incubated at 37 °C under 5% CO₂ for 24 h. The treated CD8⁺ T cells were collected from the supernatant of the co-culture system for transcriptome analysis. The total RNA of CD8⁺ T cells was extracted by TRIzol kit according to the manufacturer's instructions, and sequenced on Illumina NovaSeq 6000 sequencer (Illumina, USA) by Majorbio Biopharm Technology (Shanghai, China). The data were analyzed on the online platform of Majorbio Cloud Platform (www.majorbio.com).

Immune activation in vivo

The immune activation effect was performed on the orthotopic colon cancer-bearing *BALB/c* mice. The mice were randomly divided into 4 groups (3 mice for each group). Various formulations (anti-PD-L1, Lipo anti-PD-L1 and eLipo anti-PD-L1) were intravenously injected into the mouse at a dose of 2.3 mg anti-PD-L1/kg at day 7, 9, and 11, respectively. PBS (pH 7.4) was used as the blank control. After euthanizing the animals at day 14, tumors were harvested, cut into small pieces, and immersed in the digestion solution (containing 0.2 mg/mL hyaluronidase, 0.5 mg/mL collagenase IV, and 0.2 mg/mL of DNase) at 37 °C for 1 h. The digested cell suspensions were filtered through 70 μm filter

to obtain single cell suspensions for the following uses: (1) to evaluate the effect on the dendritic cell maturation, the single cell suspensions were stained with FITC anti-mouse CD11c, PE anti-mouse CD80, and PE-Cy7 anti-mouse CD86; (2) to observe the effect on the cytotoxic T lymphocytes (CTLs), the single cell suspensions were stained with PE-Cy7 anti-mouse CD45, FITC anti-mouse CD3e, PE anti-mouse CD4, and brilliant violet 421TM anti-mouse CD8; and (3) to explore the effect on the regulatory T cells (Treg cells), the single cell suspensions were stained with PE-Cy7 anti-mouse CD45, FITC anti-mouse CD3e, PE anti-mouse CD4, and PE anti-mouse FOXP3. The live/dead cells were discriminated by using Zombie AquaTM kit according to the manufacturer's instruction. The above samples were then analyzed by flow cytometry (Gallios, Beckman Coulter, USA) (Supplementary Fig. 22), respectively. The data were analyzed using FlowJoTM V10 software (BD Biosciences, USA).

Besides, the spleens were also harvested from the orthotopic colon cancer-bearing mice at day 14, and directly ground to cell suspensions, and filtered through 70 μ m filter to obtain single cell suspensions for the following uses: (1) to observe the effect on the cytotoxic T lymphocytes (CTLs), the single cell suspensions were stained with PE-Cy7 anti-mouse CD45, FITC anti-mouse CD3e, PE anti-mouse CD4, and brilliant violet 421TM anti-mouse CD8; (2) to evaluate TNF- α expression in CD8⁺ T cells, the single cell suspensions were stained with PE-Cy7 anti-mouse CD45, FITC anti-mouse CD3e, PE anti-mouse CD4, brilliant violet 421TM anti-mouse CD8, and APC anti-mouse TNF- α ; (3) to evaluate IFN- γ expression in CD8⁺ T cells, the single cell suspensions were stained with PE-Cy7 anti-mouse CD45, FITC anti-mouse CD3e, PE anti-mouse CD4, brilliant violet 421TM anti-mouse CD8, and PE anti-mouse IFN- γ ; and (4) to evaluate exhausted T cells (PD1^{hi}CD8⁺ T cells), the single cell suspensions were stained with PE-Cy7 anti-mouse CD45, FITC anti-mouse CD3e, PE anti-mouse CD4, brilliant violet 421TM anti-mouse CD8, and APC anti-mouse CD279. The live/dead cells were discriminated by using Zombie AquaTM kit according to the manufacturer's instruction. The above samples were then analyzed by flow cytometry (Gallios, Beckman Coulter, USA), respectively. The data were analyzed using FlowJoTM V10 software (BD Biosciences, USA).

Moreover, the CD8 expression was evaluated on the tumor tissue of the orthotopic colon cancer-bearing mice. The colon cancer-bearing mice were randomly divided into four groups (each 3 mice). Various formulations (anti-PD-L1, Lipo anti-PD-L1 and eLipo anti-PD-L1) were the same intravenously injected into the mouse at a dose of 2.3 mg anti-PD-L1/kg at day 7, 9, and 11, respectively. PBS (pH 7.4) was used as the blank control. After euthanizing the animals at day 14, tumor masses were isolated, fixed with 4% paraformaldehyde, embedded in paraffin, and sectioned, followed by immunofluorescence imaging using confocal laser scanning microscopy (TCS-SP8, Leica, Germany). Meanwhile, kidney samples of the mice were also collected and the same processed as those of tumor samples at day 14 for hematoxylin and eosin (HE) staining and Masson staining, respectively.

Therapeutic efficacy in the colon cancer-bearing mice

Orthotopic colon cancer CT-26 cells-bearing *BALB/c* mice were used for evaluating the inhibitory effect on tumor growth and the preliminary safety. The mice were randomly divided into 9 groups (5 mice for each group). Various formulations (PBS pH 7.4, anti-PD-L1, Lipo anti-PD-L1, eLipo anti-PD-L1, dox, Lipo dox, eLipo dox, Lipo anti-PD-L1 dox, and eLipo anti-PD-L1 dox) were intravenously injected into the mice at a dose of 3 mg dox/kg and/or 2.3 mg anti-PD-L1/kg at day 7, 9, and 11, respectively. To observe the inhibitory effect on tumor growth, the mice were euthanized by cervical dislocation at day 17, and tumor masses were collected for evaluating tumor weight and volume, and then photographed. The tumor volume was calculated according to the long diameter (L) and short diameter (S) of the tumor mass, and

the calculation formula was as follow:

$$\text{Volume}(\text{mm}^3) = 0.5 \times L \times S^2$$

For observing the preliminary safety, body weight of each mouse was recorded every 2 days from day 7 to day 17. Besides, 3 mice were randomly selected from the 5 mice per group at day 17. Serum samples of these 3 mice in each group were randomly collected for evaluating blood biochemical indicators, including aspartate aminotransferase (AST) and albumin (ALB). In addition, the effect of anti-PD-L1 containing formulations on the kidney was evaluated on the orthotopic colon cancer CT-26 cells-bearing mice. After various treatments (PBS pH 7.4, anti-PD-L1, Lipo anti-PD-L1, eLipo anti-PD-L1), serum samples were collected at day 17 for evaluating blood urea concentration, which was used as a blood biochemical indicator to evaluate kidney physiological function.

Orthotopic colon cancer ^{luc}CT-26 cells-bearing *BALB/c* mice were used for evaluating the survival curve and cancer progression. The mice were randomly divided into 9 groups (5 mice for each group). Various formulations (PBS pH 7.4, anti-PD-L1, Lipo anti-PD-L1, eLipo anti-PD-L1, dox, Lipo dox, eLipo dox, Lipo anti-PD-L1 dox, and eLipo anti-PD-L1 dox) were the same injected into the mice at a dose of 3 mg dox/kg and/or 2.3 mg anti-PD-L1/kg at day 7, 9, and 11, respectively. Death events were recorded every day, and the survival curve was analyzed by Kaplan-Meier survival analysis. For evaluating the progression of cancer, each mouse was intraperitoneally injected with luciferase substrate D-luciferin potassium salt (150 mg/kg), and 10 min later, the mouse was imaged by a real-time imaging system (IVIS Spectrum, PerkinElmer, USA). As tumor size was not measurable directly, the imaging observation was conducted once a week to monitor the orthotopic colon cancer ^{luc}CT-26 cells-bearing mice.

To evaluate the efficacy in the subcutaneous colon cancer *C57BL/6* mice model, both female and male colon cancer-bearing mice with MC-38 cells were randomly divided into 9 groups (6 female mice or 6 male mice for each group). Various formulations (PBS pH 7.4, anti-PD-L1, Lipo anti-PD-L1, eLipo anti-PD-L1, dox, Lipo dox, eLipo dox, Lipo anti-PD-L1 dox, and eLipo anti-PD-L1 dox) were intravenously injected into the mice at a dose of 3 mg dox/kg and/or 2.3 mg anti-PD-L1/kg at day 5, 7, and 9, respectively. Tumor volume was measured every 3 days starting from day 0 using a vernier caliper. Body weight was recorded every 2 days from day 5 to day 15. The tumor volume was calculated according to the long diameter (L) and short diameter (S) of the tumor mass, and the calculation formula was the same as above.

Statistical analysis

Statistical analysis was performed using GraphPad Prism (Version 8.0.2). All quantitative parameters were presented as mean \pm standard deviation (SD). Statistical significance was analyzed by a two-tailed unpaired Student's *t* test for comparison between two groups and by a one-way ANOVA test followed by a Turkey multiple comparisons post-test for comparison among multiple groups. Survival significance was measured by log-rank test. The sample size for analysis was as annotated in figure legends. At least three independent experiments were performed for each in vitro study, and at least five mice were included for in vivo antitumor experiments. Statistical significance was set as follows: **P* < 0.05, ***P* < 0.01, ****P* < 0.001, and *****P* < 0.0001. The details of statistical analysis for figures and supplementary figures are included in the Source Data file.

Reporting summary

Further information on research design is available in the Nature Portfolio Reporting Summary linked to this article.

Data availability

The transcriptome sequencing data generated in this study have been deposited in the NCBI Sequence Read Archive (SRR28295793, SRR28295792, SRR28295791, SRR28295790, SRR28295789, SRR28295788, SRR28295787, SRR28295786, SRR28295785), and are available at the following URLs: <https://www.ncbi.nlm.nih.gov/sra/?term=SRR28295793>; <https://www.ncbi.nlm.nih.gov/sra/?term=SRR28295792>; <https://www.ncbi.nlm.nih.gov/sra/?term=SRR28295791>; <https://www.ncbi.nlm.nih.gov/sra/?term=SRR28295790>; <https://www.ncbi.nlm.nih.gov/sra/?term=SRR28295789>; <https://www.ncbi.nlm.nih.gov/sra/?term=SRR28295788>; <https://www.ncbi.nlm.nih.gov/sra/?term=SRR28295787>; <https://www.ncbi.nlm.nih.gov/sra/?term=SRR28295786>; <https://www.ncbi.nlm.nih.gov/sra/?term=SRR28295785>.

The remaining data are available within the Article, Supplementary Information or Source Data file. The raw numbers for charts and graphs are available in the Source Data file whenever possible. Source data are provided with this paper.

References

- Lichtenstern, C. R. et al. Immunotherapy, inflammation and colorectal cancer. *Cells* **9**, 618 (2020).
- Labianca, R. et al. Colon cancer. *Crit. Rev. Oncol. Hematol.* **74**, 106–133 (2010).
- Stein, A. et al. Current standards and new trends in the primary treatment of colorectal cancer. *Eur. J. Cancer* **47**, S312–S314 (2011).
- Cunningham, D. et al. Colorectal cancer. *Lancet* **375**, 1030–1047 (2010).
- Jiang, Y. et al. Global pattern and trends of colorectal cancer survival: a systematic review of population-based registration data. *Cancer Biol. Med.* **19**, 175–186 (2021).
- Wolchok, J. D. et al. Nivolumab plus ipilimumab in advanced melanoma. *N. Engl. J. Med.* **369**, 122–133 (2013).
- Topalian, S. L. et al. Safety, activity, and immune correlates of anti-PD-1 antibody in cancer. *N. Engl. J. Med.* **366**, 2443–2454 (2012).
- Herbst, R. S. et al. Predictive correlates of response to the anti-PD-L1 antibody MPDL3280A in cancer patients. *Nature* **515**, 563–567 (2014).
- Robert, C. et al. Pembrolizumab versus ipilimumab in advanced melanoma. *N. Engl. J. Med.* **372**, 2521–2532 (2015).
- Delivanis, D. A. et al. Pembrolizumab-induced thyroiditis: comprehensive clinical review and insights into underlying involved mechanisms. *J. Clin. Endocrinol. Metab.* **102**, 2770–2780 (2017).
- Ribas, A. et al. Cancer immunotherapy using checkpoint blockade. *Science* **359**, 1350–1355 (2018).
- Sharma, P. et al. The future of immune checkpoint therapy. *Science* **348**, 56–61 (2015).
- Pardoll, D. M. The blockade of immune checkpoints in cancer immunotherapy. *Nat. Rev. Cancer* **12**, 252–264 (2012).
- Masugi, Y. et al. Tumour CD274 (PD-L1) expression and T cells in colorectal cancer. *Gut* **66**, 1463–1473 (2017).
- Andre, T. et al. Pembrolizumab in microsatellite-instability-high advanced colorectal cancer. *N. Engl. J. Med.* **383**, 2207–2218 (2020).
- Lenz, H. J. et al. First-line nivolumab plus low-dose ipilimumab for microsatellite instability-high/mismatch repair-deficient metastatic colorectal cancer: the phase II CheckMate 142 study. *J. Clin. Oncol.* **40**, 161–170 (2022).
- Cercek, A. et al. PD-1 blockade in mismatch repair-deficient, locally advanced rectal cancer. *N. Engl. J. Med.* **386**, 2363–2376 (2022).
- Mettu, N. B. et al. Assessment of capecitabine and bevacizumab with or without atezolizumab for the treatment of refractory metastatic colorectal cancer: a randomized clinical trial. *JAMA Netw. Open* **5**, e2149040 (2022).
- Antonioti, C. et al. Upfront FOLFOXIRI plus bevacizumab with or without atezolizumab in the treatment of patients with metastatic colorectal cancer (AtezoTRIBE): a multicentre, open-label, randomised, controlled, phase 2 trial. *Lancet Oncol.* **23**, 876–887 (2022).
- Eng, C. et al. Atezolizumab with or without cobimetinib versus regorafenib in previously treated metastatic colorectal cancer (IMblaze370): a multicentre, open-label, phase 3, randomised, controlled trial. *Lancet Oncol.* **20**, 849–861 (2019).
- Hellmann, M. D. et al. Phase Ib study of atezolizumab combined with cobimetinib in patients with solid tumors. *Ann. Oncol.* **30**, 1134–1142 (2019).
- Diaz, L. A., Jr. et al. Pembrolizumab versus chemotherapy for microsatellite instability-high or mismatch repair-deficient metastatic colorectal cancer (KEYNOTE-177): final analysis of a randomised, open-label, phase 3 study. *Lancet Oncol.* **23**, 659–670 (2022).
- Huyghe, N. et al. Immunotherapy with immune checkpoint inhibitors in colorectal cancer: what is the future beyond deficient mismatch-repair tumours? *Gastroenterol. Rep. (Oxf.)* **8**, 11–24 (2020).
- Suk, J. S. et al. PEGylation as a strategy for improving nanoparticle-based drug and gene delivery. *Adv. Drug Deliv. Rev.* **99**, 28–51 (2016).
- Pasut, G. et al. State of the art in PEGylation: the great versatility achieved after forty years of research. *J. Control Release* **161**, 461–472 (2012).
- Maute, R. L. et al. Engineering high-affinity PD-1 variants for optimized immunotherapy and immuno-PET imaging. *Proc. Natl Acad. Sci. USA* **112**, E6506–E6514 (2015).
- Francisco, L. M. et al. The PD-1 pathway in tolerance and autoimmunity. *Immunol. Rev.* **236**, 219–242 (2010).
- Chen, J. M. et al. Identification of the active site of legumain links it to caspases, clostripain and gingipains in a new clan of cysteine endopeptidases. *FEBS Lett.* **441**, 361–365 (1998).
- Dall, E. et al. Mechanistic and structural studies on legumain explain its zymogenicity, distinct activation pathways, and regulation. *Proc. Natl Acad. Sci. USA* **110**, 10940–10945 (2013).
- Miller, G. et al. Asparagine endopeptidase is required for normal kidney physiology and homeostasis. *FASEB J.* **25**, 1606–1617 (2011).
- Liu, C. et al. Overexpression of legumain in tumors is significant for invasion/metastasis and a candidate enzymatic target for prodrug therapy. *Cancer Res.* **63**, 2957–2964 (2003).
- Chen, Y. J. et al. Peptide-based MRI contrast agent and near-infrared fluorescent probe for intratumoral legumain detection. *Biomaterials* **35**, 304–315 (2014).
- Li, N. et al. Effects of legumain as a potential prognostic factor on gastric cancers. *Med Oncol.* **30**, 621 (2013).
- Shah, S. et al. Liposomes: advancements and innovation in the manufacturing process. *Adv. Drug Deliv. Rev.* **154–155**, 102–122 (2020).
- Large, D. E. et al. Liposome composition in drug delivery design, synthesis, characterization, and clinical application. *Adv. Drug Deliv. Rev.* **176**, 113851 (2021).
- Carvalho, P. M. et al. Application of light scattering techniques to nanoparticle characterization and development. *Front. Chem.* **6**, 237 (2018).
- Gotz, M. G. et al. Aza-peptidyl Michael acceptors. A new class of potent and selective inhibitors of asparaginyl endopeptidases (legumains) from evolutionarily diverse pathogens. *J. Med. Chem.* **51**, 2816–2832 (2008).
- Ovat, A. et al. Aza-peptidyl Michael acceptor and epoxide inhibitors-potent and selective inhibitors of *Schistosoma mansoni* and *Ixodes ricinus* legumains (asparaginyl endopeptidases). *J. Med. Chem.* **52**, 7192–7210 (2009).
- Niestroj, A. J. et al. Inhibition of mammalian legumain by Michael acceptors and AzaAsn-halomethylketones. *Biol. Chem.* **383**, 1205–1214 (2002).

40. Ekici, O. D. et al. Aza-peptide Michael acceptors: a new class of inhibitors specific for caspases and other clan CD cysteine proteases. *J. Med. Chem.* **47**, 1889–1892 (2004).
41. Larue, L. et al. tLyp-1: A peptide suitable to target NRP-1 receptor. *Bioorg. Chem.* **130**, 106200 (2023).
42. Ganesh, K. et al. Immunotherapy in colorectal cancer: rationale, challenges and potential. *Nat. Rev. Gastroenterol. Hepatol.* **16**, 361–375 (2019).
43. Liu, C. et al. Combining radiation and the ATR inhibitor berzosertib activates STING signaling and enhances immunotherapy via inhibiting SHP1 function in colorectal cancer. *Cancer Commun. (Lond.)* **43**, 435–454 (2023).
44. Mandal, R. et al. Genetic diversity of tumors with mismatch repair deficiency influences anti-PD-1 immunotherapy response. *Science* **364**, 485–491 (2019).
45. Ho, W. W. et al. Dendritic cell paucity in mismatch repair-proficient colorectal cancer liver metastases limits immune checkpoint blockade efficacy. *Proc. Natl Acad. Sci. USA* **118**, e2105323118 (2021).
46. Liu, Z. et al. Legumain protease-activated TAT-liposome cargo for targeting tumours and their microenvironment. *Nat. Commun.* **5**, 4280 (2014).
47. Zhao, L. et al. Structural analysis of asparaginyl endopeptidase reveals the activation mechanism and a reversible intermediate maturation stage. *Cell Res.* **24**, 344–358 (2014).
48. Fang, J. et al. Exploiting the dynamics of the EPR effect and strategies to improve the therapeutic effects of nanomedicines by using EPR effect enhancers. *Adv. Drug Deliv. Rev.* **157**, 142–160 (2020).
49. Maeda, H. Toward a full understanding of the EPR effect in primary and metastatic tumors as well as issues related to its heterogeneity. *Adv. Drug Deliv. Rev.* **91**, 3–6 (2015).
50. Soker, S. et al. Neuropilin-1 is expressed by endothelial and tumor cells as an isoform-specific receptor for vascular endothelial growth factor. *Cell* **92**, 735–745 (1998).
51. Latil, A. et al. VEGF overexpression in clinically localized prostate tumors and neuropilin-1 overexpression in metastatic forms. *Int. J. Cancer* **89**, 167–171 (2000).
52. Hoos, A. Development of immuno-oncology drugs—from CTLA4 to PD1 to the next generations. *Nat. Rev. Drug Discov.* **15**, 235–247 (2016).
53. Mahoney, K. M. et al. Combination cancer immunotherapy and new immunomodulatory targets. *Nat. Rev. Drug Discov.* **14**, 561–584 (2015).

Acknowledgements

The authors thank L. Su, Y. Liu, Y. R. Jia, W. Wang, X. Yuan, J. Liu, W. Ma, X. J. Zou, J. Li, J. Wang, and W. T. Li from Peking University Health Science Center for their professional technical assistance and guidance. This work was supported in part by the National Natural Science Foundation

of China (No. 82173752 W. L. Lu) and National Natural Science Foundation of China (No. 81874303 W. L. Lu).

Author contributions

W. L. L. conceived and supervised the project. Y. X. L., Y. X., Y. L. C., J. L. W., H. X. F., and M. J. W. completed the experiments. Y. X. L., J. L. D., C. J. B., Y. X. R., P. S. L., Q. L., J. R. X., M. J., Y. C. M., Y. W., J. W. L., and G. L. W. analyzed the data. Y. X. L. wrote the manuscript. W. L. L. revised the manuscript. All the authors contributed to the discussion and revision of the manuscript.

Competing interests

The authors declare no competing interests.

Additional information

Supplementary information The online version contains supplementary material available at <https://doi.org/10.1038/s41467-025-57965-6>.

Correspondence and requests for materials should be addressed to Wanliang Lu.

Peer review information *Nature Communications* thanks Yoshihiro Morimoto and the other anonymous reviewer(s) for their contribution to the peer review of this work. A peer review file is available.

Reprints and permissions information is available at <http://www.nature.com/reprints>

Publisher's note Springer Nature remains neutral with regard to jurisdictional claims in published maps and institutional affiliations.

Open Access This article is licensed under a Creative Commons Attribution-NonCommercial-NoDerivatives 4.0 International License, which permits any non-commercial use, sharing, distribution and reproduction in any medium or format, as long as you give appropriate credit to the original author(s) and the source, provide a link to the Creative Commons licence, and indicate if you modified the licensed material. You do not have permission under this licence to share adapted material derived from this article or parts of it. The images or other third party material in this article are included in the article's Creative Commons licence, unless indicated otherwise in a credit line to the material. If material is not included in the article's Creative Commons licence and your intended use is not permitted by statutory regulation or exceeds the permitted use, you will need to obtain permission directly from the copyright holder. To view a copy of this licence, visit <http://creativecommons.org/licenses/by-nc-nd/4.0/>.

© The Author(s) 2025